

# Identification and functional characterization of the putative members of the CTDK-1 kinase complex as regulators of growth and development in *Aspergillus nidulans* and *Aspergillus fumigatus*

Z. Agirrezabala,<sup>1</sup> X. Guruceaga,<sup>2</sup> A. Martin-Vicente,<sup>2</sup> A. Otamendi,<sup>1</sup> A. Fagoaga,<sup>1</sup> J. R. Fortwendel,<sup>2</sup> E. A. Espeso,<sup>3</sup> O. Etxebeste<sup>1</sup>

**AUTHOR AFFILIATIONS** See affiliation list on p. 26.

**ABSTRACT** Asexual spores are the main vehicle used by fungi to disperse to new niches. The Eurotiomycete *Aspergillus nidulans* is the main reference for the study of the genetic/molecular control of asexual development. In this species, Flb proteins control the expression of the master gene *brlA*, and thus, loss-of-function mutations in *flb* (upstream developmental activation [UDA]) genes block *brlA* transcription and, consequently, the production of conidiophores, the structures bearing asexual spores known as conidia. However, the aconidial phenotype of specific *flb* mutants, such as that of the  $\Delta flbB$  strain, is reverted under salt-stress conditions. Previously, we generated a collection of second-site mutants of  $\Delta flbB$  unable to conidiate on culture medium supplemented with  $\text{NaH}_2\text{PO}_4$  (0.65 M). Here, we identified a Gly347Stop mutation within *flpA* as responsible for the FLIP57 phenotype and characterized the role of the putative cyclin FlpA and the remaining putative components of the C-terminal domain kinase-1 (CTDK-1) complex in *A. nidulans* and *Aspergillus fumigatus*. FlpA, Stk47, and FlpB are necessary (i) for timely germination, (ii) in the transition from metulae to phialides (the cells generating conidia) during conidiophore development, and (iii) for the development of sexual structures (cleistothecia) in *A. nidulans*. The three proteins are nuclear, and the nucleoplasmic localization of Stk47 depends on the activity of FlpA, which correlates with the retention of Stk47 by FlpA in pull-down assays. Overall, this work links the putative CTDK-1 complex of aspergilli with growth and developmental control. Identification of a mutation in *flpA* as inhibitor of conidiation in *A. nidulans* and functional characterization of FlpA, Stk47 and FlpB as putative members of the C-terminal domain kinase complex CTDK-1 in *A. nidulans* and *A. fumigatus*.

**IMPORTANCE** *Aspergillus fumigatus* has been included by the World Health Organization in the priority list of fungal pathogens because (i) it causes 90% of invasive aspergillosis cases, with a high mortality rate, and (ii) infections are becoming increasingly resistant to azole antifungals. *A. nidulans* is an opportunistic pathogen and a saprotroph which has served during the last 80 years as a reference system for filamentous fungi. Here, we characterized the role in morphogenesis and development of the putative transcriptional cyclin/kinase complex CTDK-1 in both aspergilli. The null mutants of the corresponding genes showed delayed germination, aberrant conidiophore development, and inhibition of cleistothecia production. While in higher eukaryotes this complex is formed only by a cyclin and a kinase, the fungal complex would incorporate a fungal-specific third component, FlpB, which would enable the interaction between the kinase (Stk47) and the cyclin (FlpA) and may be used as a target for antifungals.

**Editor** Gustavo H. Goldman, Universidade de Sao Paulo, Sao Paulo, Brazil

Address correspondence to O. Etxebeste, oier.echeveste@ehu.eus.

Z. Agirrezabala and X. Guruceaga contributed equally to this article. The order of these two authors was determined alphabetically and with their consent.

The authors declare no conflict of interest.

See the funding table on p. 27.

**Received** 12 September 2023

**Accepted** 3 October 2023

**Published** 9 November 2023

Copyright © 2023 Agirrezabala et al. This is an open-access article distributed under the terms of the [Creative Commons Attribution 4.0 International license](https://creativecommons.org/licenses/by/4.0/).

**KEYWORDS** filamentous fungi, *Aspergillus nidulans*, *Aspergillus fumigatus*, vegetative growth, asexual development, conidiation, sexual development, stress response, cyclin, kinase, CTDK-1, RNA polymerase II

*Aspergilli* constitute an important genus of filamentous fungi. Taxonomically, the genus is located within the phylum Ascomycota, subphylum Pezizomycotina, and the class of Eurotiomycetes. It is composed of hundreds (~350) of species (1). Some of them are pathogens of fruits, seeds, animals, and humans. For example, *Aspergillus fumigatus* is the main agent causing invasive aspergillosis (2). Other *aspergilli* are used in industry as a source of valuable products (3, 4). *Aspergillus* species can reproduce sexually or asexually (5). Sexual development has been described in a subset of species of this genus, but sequencing of *Aspergillus* genomes has uncovered that the presence of genes coding main regulators of sex is a general trend (1). Sexual reproduction is based on meiotic cell divisions, generating spores with combinations of the genetic content of the parentals (6, 7). Asexual reproduction is based on mitosis, producing spores with an identical genetic content. This explains why sexual reproduction is mainly directed to the interchange of genetic material, while the main aim of asexual development is dispersal.

Spores germinate under favorable environmental conditions. Polar growth and branching of germlings generate mature hyphae, while fusion of hyphae through anastomosis generates the mycelium, the structure specialized in substrate colonization (8). Depending on the stimulus (O<sub>2</sub> or CO<sub>2</sub>, light/darkness, nutrient availability/starvation, salt or osmotic stress, presence/absence of specific metabolites) (9), asexual or sexual developmental programs will be activated or repressed. Those spores disperse again to new niches, initiating new life cycles.

One of the main model organisms within the genus *Aspergillus* is *Aspergillus nidulans*. Several features make this species a suitable reference organism: fast growth rates at laboratory conditions, the fact that it is not a pathogen, the possibility of carrying out sexual crosses in short periods of time, the amenability for genetic manipulation, and the availability of a vast array of standardized cellular and molecular techniques (10). Together with the Sordariomycete *Neurospora crassa*, *A. nidulans* is the main reference species in the study of developmental programs (3, 10, 11), since most of the known regulators of sexual and asexual development were identified and characterized for the first time in *A. nidulans* (2). Asexual spores of *A. nidulans* are known as conidia since they are produced by localized budding and subsequent constriction from an external sporogenous cell, called the phialide (12). Phialides and conidia are the last cell types produced in the asexual developmental cycle, giving rise to multi-cellular structures called conidiophores. Each *A. nidulans* conidiophore, and the same holds true for *A. fumigatus*, produces thousands of conidia, and each colony generates millions of conidiophores on solid culture (9, 10, 13–15).

In his seminal works, Timberlake estimated that more than a thousand mRNAs increased their concentration after the induction of conidiophore development (16). To date, the number of identified and functionally characterized proteins with a role in asexual development is far from this estimation. These regulators have been classified into signal transducers, central regulators, repressors, and balancers (9, 17). There are complex functional and genetic relationships among these groups of regulators, as well as between them and regulators of other cellular processes such as polar growth, sexual development, secondary metabolism, or cell death. A simplified model describes the activity of two main pathways (18). UDA pathways are signal transduction pathways involved in the inhibition of polar growth of hyphae and the decision of whether to induce or not, depending on extracellular and intracellular stimuli, asexual development. There are at least three UDA subpathways, which are defined by *flbA*, *flbB/flbD/flbE*, and *flbC*, respectively. FlbB, FlbC, and FlbD are transcription factors and play an important role in the induction of the expression of *brlA*. In fact, *brlA* is the central gene in this model, since its expression is controlled by UDA-s, and then, BrlA controls the expression

of central developmental pathway (CDP) genes, which regulate the formation of most of the cell types of the conidiophore (9, 17, 19). As mentioned above, there are known repressors of *brlA* expression, which act at two levels: repressors that also activate sexual development and those that repress *brlA* expression once asexual development has been completed (20–24).

Due to their role in the control of *brlA* expression, deletion or loss-of-function mutations in UDA genes inhibit or delay conidiation. Mutants show an aconidial phenotype known as *fluffy* (14). An example is the  $\Delta flbB$  mutant, in which the CDP pathway is blocked. Nevertheless, the *fluffy* phenotype of the null *flbB* mutant is reverted under specific stress conditions, such as supplementation of the standard solid *Aspergillus* minimal medium (AMM) with high concentrations (above 0.5 M) of  $\text{NaH}_2\text{PO}_4$  (25–27). In a previous work, we took advantage of this phenotype and mutagenized through UV light conidia of a  $\Delta flbB$  strain with the aim of isolating second-site mutants unable to conidiate when cultured on AMM supplemented with 0.65 M  $\text{NaH}_2\text{PO}_4$  (27). These mutants were named as FLIP (*fluffy* in phosphate mutants).

In this work, mutants FLIP57 and FLIP76 have been characterized. Identification of the mutations causing their phenotypes led to the characterization of AN10640/FlpA (*fluffy* in phosphate A) as a putative cyclin required in the transition from metulae to phialides during conidiophore development. Fluorescence microscopy suggested that its localization is cell cycle dependent, being located in the nucleoplasm in the interphase but not during mitosis. The same phenotype and subcellular localization were observed for its putative interaction partners AN8190/Stk47, a cyclin-dependent kinase (CDK), and AN6312/FlpB, a homolog of *Schizosaccharomyces pombe* Ctk3. Specific dependencies were described among these three proteins for nuclear accumulation and immunodetection patterns. Besides development, germination and radial growth were also remarkably affected in the null mutants of *flpA*, *stk47*, or *flpB* both in *A. nidulans* and *A. fumigatus*. Overall, results suggest that the activity of the putative C-terminal domain kinase-1 (CTDK-1) complex in the genus *Aspergillus* is required in multiple cellular processes, participating in the coordination of growth and developmental programs.

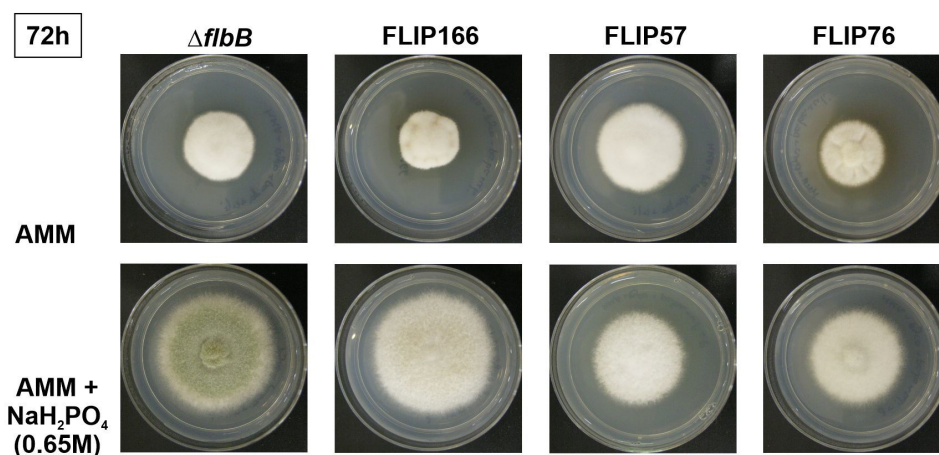
## RESULTS

### Sequencing and analysis of FLIP57 and FLIP76 genomes

In a previous work, 80 second-site mutants of  $\Delta flbB$  unable to conidiate on AMM supplemented with 0.65 M  $\text{NaH}_2\text{PO}_4$  (FLIP mutants) were grouped into seven phenotypic groups (27). We determined that the mutant phenotype of FLIP166, which belonged to the group of FLIP mutants with a totally aconidial phenotype under phosphate stress conditions, was caused by a mutation in *AN1459/pmtC* (27, 28). Eight additional FLIP mutants were selected (Fig. S1), their genomic DNA extracted and *pmtC* sequenced. None of the FLIP mutants analyzed bore a mutation in this gene, showing that their phenotypes were not caused by mutant *pmtC* alleles. Genomic DNA samples of FLIP57 and FLIP76 (Fig. 1A) were sequenced and compared to the reference FGSC4 genome, the FLIP166 genome, and *A. nidulans* transcriptomes (see Materials and Methods; see File S1) (23, 27, 29). Four and three exonic candidate mutations were identified in FLIP57 and FLIP76, respectively (Fig. 1B). However, in FLIP76, an exonic mutation was identified in *AN5717/kapl*, leading to a premature stop codon (R557E+8-Stop; Kapl is 1,095 amino acids long; File S1; Fig. 1B). Since we previously described that the double  $\Delta kapl; \Delta flbB$  mutant was completely aconidial under stress conditions induced by the addition of 0.5 M  $\text{NaH}_2\text{PO}_4$  (30), we concluded that the FLIP76 phenotype was caused by the additive effect of *flbB* deletion and a loss-of-function mutation in *kapl*. Consequently, we discarded FLIP76 and continued the analysis with FLIP57.

In this second mutant, out of four exonic mutations identified, *AN6932* and *AN7856* (File S1) were discarded because the corresponding null mutant did not show a defect in conidiation (31) or because the gene showed very low expression levels (*AN7856*). *AN7842* was also discarded because, despite the low expression levels, RNA-seq reads suggested that it is not correctly annotated. Thus, the analysis was focused on the

A



B

Candidate gene	DNA mutation	Protein change	Description
<b>FLIP57</b>			
<i>AN6932/uapA</i>	ATG400ATA	Met400Ile	High-capacity, high-affinity uric acid-xanthine permease
<i>AN7856</i>	TTG253TTT	Leu253Phe	Has domain(s) with predicted enoyl-[acyl-carrier-protein] reductase (NADH) activity, fatty acid synthase activity
<i>AN7842</i>	CTG120CCG	Leu120Pro	Protein of unknown function
<i>AN10640</i>	GGA347TGA	Gly347Stop	Ortholog(s) have cyclin-dependent protein serine/threonine kinase activator activity
<b>FLIP76</b>			
<i>AN12237/abpA</i>	GAA742GCA	Glu742Ala	Putative actin-binding protein of the cortical actin patches involved in endocytosis
<i>AN5221</i>	ATG1097ATC	Met1097Ile	ORF uncharacterized
<i>AN5717/kapl</i>	CGA557GA	Arg557Glu + 8 + Stop	Non-essential karyopherin family protein; required for normal hyphal growth and conidial development

**FIG 1** Mutations found in FLIP57 and FLIP76. (A) Phenotypes of mutants FLIP57 and FLIP76 after 72 hours of culture at 37°C in AMM (row 1) or AMM supplemented with 0.65 M NaH<sub>2</sub>PO<sub>4</sub> (row 2). A parental *ΔflbB* and the mutant FLIP166 (27) were used as controls. (B) Mutations found in the genomes of FLIP57 and FLIP76, which could be responsible for the corresponding FLIP phenotypes.

mutation found in *AN10640* because (i) RNA-seq data showed that the annotation of exons and introns was correct; (ii) it showed moderate expression levels (see below); and (iii) the gene is predicted to encode a cyclin. That would link the control of asexual development with the control of the cell cycle, transcription, and/or additional cellular processes.

#### A point mutation corresponding to a Gly347Stop truncation in *AN10640/FlpA* caused the FLIP57 phenotype

*AN10640* is located in chromosome V (coordinates 1,323,461–1,325,516, coding strand) and is composed of five exons and four introns. The G-T mutation of FLIP57 is located

in exon 5 and modifies the codon in the position 347 (GGA, Gly) by a stop signal (TGA, Gly347Stop) (Fig. 2A). Since the corresponding protein is predicted to be 392 amino acids long, the FLIP57 mutation would cause the truncation of the last 45 amino acids (Fig. 2A). RNA-seq data showed that, in the culture conditions and genetic backgrounds analyzed by others in *A. nidulans* (reviewed in reference 32), the position and extension of introns of *AN10640* matched the FungiDB annotations. Furthermore, RNA-seq data, including FPKM values for wild type and the null *flbB* backgrounds before (VG) and after (AD, 5 hours) the induction of asexual development (23, 33), showed moderate expression levels in all conditions/backgrounds analyzed, with no remarkable induction/inhibition of *AN10640* in any of the samples (Fig. 2B). The Interpro server predicted the presence of a cyclin-like domain (IPR013763, amino acids 59–263; Fig. 2A), which is described to be found in cyclins but also in transcription factor IIB and in the retinoblastoma tumor suppressor (34–36). The FungiDB database described that orthologs of *AN10640* have roles in positive regulation of septation initiation signaling, regulation of phosphorylation of RNA polymerase II C-terminal domain, and trimeric positive transcription elongation factor complex b localization. The FLIP57 mutation is located outside of this putative cyclin-like domain.

To confirm that the mutation Gly347Stop in *AN10640* (the gene was named as *flpA*, *fluffy* in phosphate A) was the cause of the FLIP57 phenotype, protoplasts of this strain and those of its parental  $\Delta flbB$  strain were transformed with *flpA::ha<sub>3x</sub>::pyrG<sup>Afum</sup>*, *flpA<sup>(Gly347Stop)</sup>::ha<sub>3x</sub>::pyrG<sup>Afum</sup>*, *flpA::gfp::pyrG<sup>Afum</sup>*, or *flpA<sup>(Gly347Stop)</sup>::gfp::pyrG<sup>Afum</sup>* constructs (Fig. 2C). The insertion of the mutant constructs in the null *flbB* parental caused an inhibition of conidiation in AMM supplemented with 0.5 M NaH<sub>2</sub>PO<sub>4</sub>, while the wild-type constructs did not alter the  $\Delta flbB$  phenotype. Inversely, the wild-type constructs reverted the FLIP57 phenotype under phosphate stress. No difference was observed between *flpA::ha<sub>3x</sub>* and *flpA::gfp* counterparts, suggesting that the size of the 3'-tag is not detrimental to FlpA activity. On the contrary, the mutant construct *flpA<sup>(Gly347Stop)</sup>::gfp::pyrG<sup>Afum</sup>* did not revert the FLIP57 phenotype under phosphate stress (Fig. 2C). These results confirmed the aforementioned hypothesis.

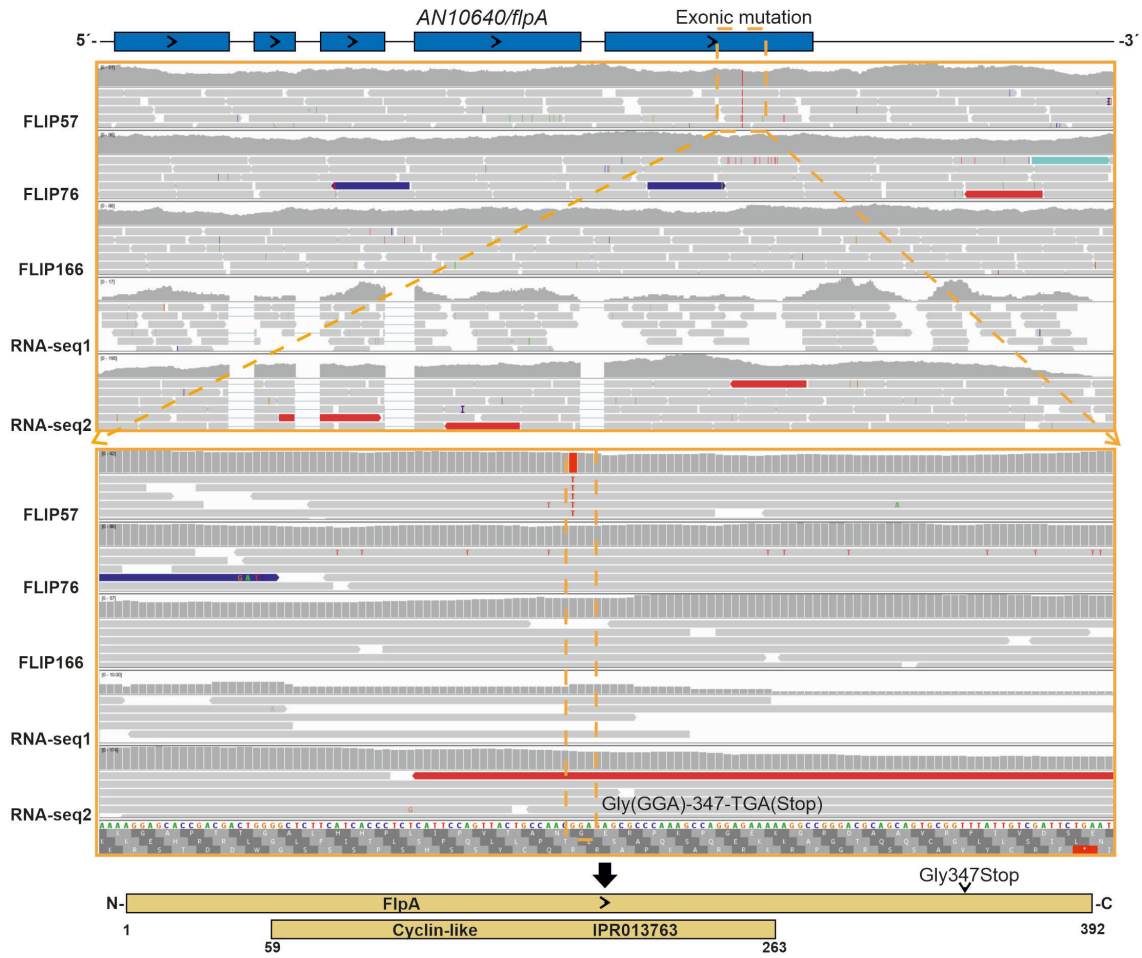
## FlpA and its putative interactors Stk47/AN8190 and FlpB/AN6312 are widely conserved in the kingdom Fungi

Paolillo and colleagues carried out a deep bioinformatics and phylogenetic analysis of *A. nidulans* cyclins (34). They classified *AN10640* within group III cyclins, as a T/K-like cyclin, as was *AN4981/PchA*. To determine the conservation pattern of FlpA in the fungal kingdom, we carried out BLAST analyses to identify putative ortholog sequences. Table S1 shows the taxonomy of the species corresponding to the FlpA hits analyzed, the length of the hit, score and *e* values, the query coverage, and the result (first sequence) of the confirmatory reverse retrieval of each hit sequence at the FungiDB database. Only hits giving *AN10640/FlpA* as the first sequence in this confirmatory reverse retrieval were considered. Overall, the values given in Table S1, together with the phylogenetic tree in Fig. 3A, show that FlpA is widely conserved in the kingdom Fungi.

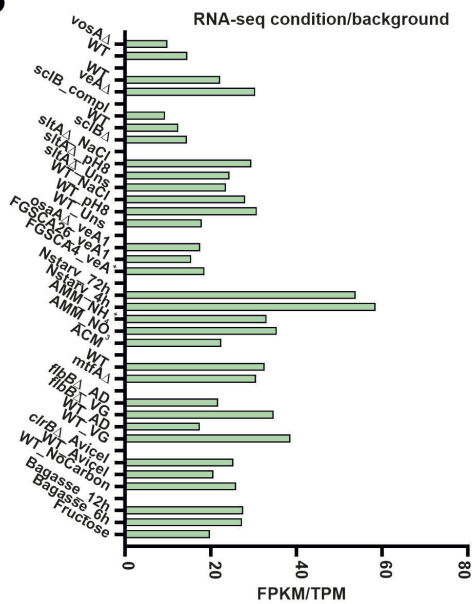
Xie and colleagues have recently determined the structure of the *Schizosaccharomyces pombe* ortholog of FlpA, Ctk2, as part of the trimeric CTDK-1 (C-terminal domain [CTD] kinase I) complex (37). CTDK-1 acts as the primary RNA polymerase II CTD Ser2 kinase complex. The Swiss-Model website modeled FlpA (from His26 to Lys374; Model 7jv7.1.B was taken as the reference; sequence identity of 18.67%) (37), with higher confidence, as expected, in the cyclin-like domain than in the case of the C-terminus (Fig. 3D; Fig. S2A). Since it corresponded to a stop signal, Dynamut (38) was unable to predict the hypothetical effect of the FLIP57 mutation in the structure of *AN10640*.

The remaining two components of the CTDK-1 complex in *S. pombe* are Ctk1, a cyclin-dependent kinase, and Ctk3, the latter being a Ctk1 activator and contributing to the assembly of the complex by interacting with Ctk1 and Ctk2 (37). The *A. nidulans* ortholog of Ctk1 is *AN8190/Stk47* (39), while that of Ctk3 is *AN6312/FlpB*. Exons and introns of both genes were annotated correctly in the FungiDB database (not shown).

**A**



**B**



**C**

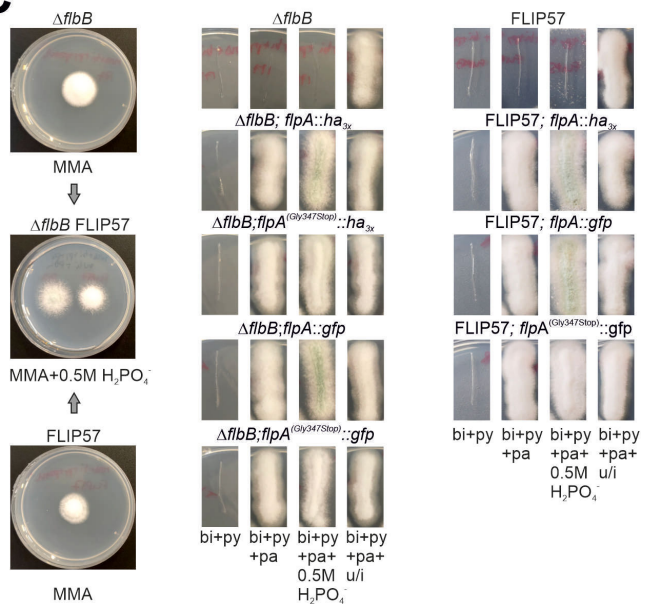


**FIG 2** A mutation within *AN10640/flpA* causes the FLIP57 phenotype. (A) Annotation of *AN10640/flpA* and analysis of the mutation causing the FLIP57 phenotype. The locus *flpA* was compared in FLIP57, FLIP76, and FLIP166 genetic backgrounds and with transcriptomes of a null *flbB* strain (RNA-seq1) and a null *sitA* strain (RNA-seq2). FLIP57 bore a mutation in the last exon of *AN10640*, which led to the substitution of the codon for Gly347 by a stop (Continued on next page)

**FIG 2** (Continued)

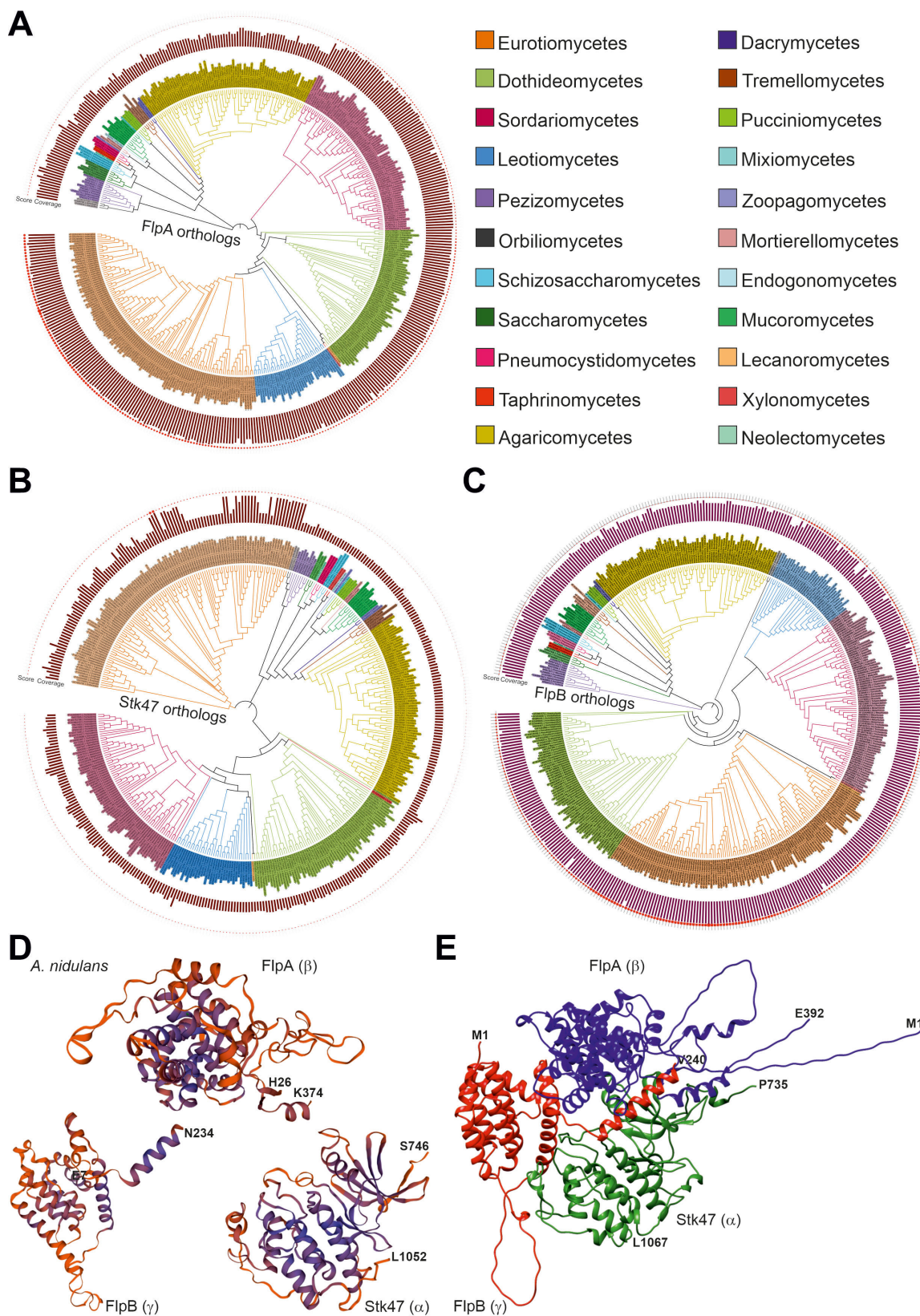
codon (loss of the last 45 amino acids). The identified mutation is outside the cyclin-like domain (IPR013763, amino acids 59–263). (B) FPKM or TPM values for *AN10640/flpA* in the multiple RNA-seq experiments available for *A. nidulans* (see references within reference 32). (C) Confirmation of the Gly347Stop truncation within *AN10640/flpA* as the mutation causing the FLIP57 phenotype. (Left) Phenotypes of FLIP57 and its parental  $\Delta flbB$  strain on AMM and AMM supplemented with 0.5 M  $\text{NaH}_2\text{PO}_4$ . (Middle) Transformants of  $\Delta flbB$  protoplasts with the synthetic DNA constructs *flpA::ha<sub>3x</sub>::pyrG<sup>Afum</sup>*, *flpA<sup>(Gly347Stop)</sup>::ha<sub>3x</sub>::pyrG<sup>Afum</sup>*, *flpA::gfp::pyrG<sup>Afum</sup>* or *flpA<sup>(Gly347Stop)</sup>::gfp::pyrG<sup>Afum</sup>*. (Right) Transformants of FLIP57 protoplasts with the synthetic DNA constructs *flpA::ha<sub>3x</sub>::pyrG<sup>Afum</sup>*, *flpA::gfp::pyrG<sup>Afum</sup>* or *flpA<sup>(Gly347Stop)</sup>::gfp::pyrG<sup>Afum</sup>*.

Table S1 includes more than 400 fungal species containing FlpA, Stk47, and FlpB (see below) orthologs, representing 22 classes within the phyla Ascomycota, Basidiomycota, and Mucoromycota (Fig. 3B and C). The Swiss-Model website modeled both proteins taking, as in the case of FlpA, PDB structure 7jv7.1 as the reference (subunits  $\alpha$  and  $\gamma$ , respectively, for Stk47 and FlpB; much lower coverage in the case of Stk47, from Ser746 to Leu1052; from Glu7 to Asn234 in the case of FlpB) (Fig. 3D; Fig S2B and C). ColabFold predicted the structure of a putative complex formed by the three *A. nidulans* proteins (full-length versions of FlpA and FlpB were used as queries and the fragment from Pro735 to Leu1067 in the case of Stk47, based in this latter case on the Swiss-Model prediction). The model in Fig. 3E shows that FlpB would interact with both FlpA and Stk47, enabling the assembly of the complex, as has been described in *S. pombe* (see the structure in Fig. S2D) (37). Overall, bioinformatics results strongly suggest that CTDK-1 is a widely conserved trimeric complex in the kingdom Fungi, while in *Homo sapiens*, there is no Ctk3 ortholog (37) (see Discussion).

### Deletion of *flpA* causes a decrease in radial growth and conidial yield, while truncation of the last 45 amino acids of FlpA has negligible effects in a wild-type background

To functionally characterize the role of FlpA in growth and development of *A. nidulans*, a null *flpA* mutant was generated, both in wild-type and  $\Delta flbB$  genetic backgrounds. Wild-type protoplasts were also transformed with wild-type and mutant (Gly347Stop) *flpA::ha<sub>3x</sub>::pyrG<sup>Afum</sup>* constructs and also a wild-type *flpA::gfp::pyrG<sup>Afum</sup>* construct (see Materials and Methods). Phenotypes of selected strains were analyzed in solid AMM and AMM supplemented with 0.5 M  $\text{NaH}_2\text{PO}_4$  (Fig. 4A). First, we observed that, after 72 hours of culture at 37°C, deletion of *flpA* caused a significant inhibition in radial extension, both in wild-type and null *flbB* backgrounds, and mainly in AMM supplemented with 0.5 M  $\text{NaH}_2\text{PO}_4$  (Fig. 4A through C). The average growth rates from 48 to 96 hours of culture were  $0.027 \pm 0.004$  and  $0.025 \pm 0.003$  cm/hour for wild-type and  $\Delta flbB$  parentals in medium supplemented with sodium dihydrogen phosphate. The values for the null *flpA* and double-null  $\Delta flpA;\Delta flbB$  strains were  $0.012 \pm 0.003$  cm/hour and  $0.012 \pm 0.001$  cm/hour, respectively, in the same culture medium ( $n = 3$  for each strain,  $P = 0.006$  and  $0.004$  for each null mutant compared to the parental strain). Furthermore, compared to the null *flbB* parental, the strain that integrated the *flpA<sup>(Gly347Stop)</sup>::ha<sub>3x</sub>::pyrG<sup>Afum</sup>* construct in this background showed only a minor decrease in the growth rate ( $0.023 \pm 0.004$  cm/h,  $n = 3$ ,  $P = 0.629$ ).

The strain that integrated the *flpA<sup>(Gly347Stop)</sup>::ha<sub>3x</sub>::pyrG<sup>Afum</sup>* construct (wild-type background) showed no inhibition of conidia production compared to the reference strain ( $6.17 \times 10^7 \pm 1.45 \times 10^7$  and  $3.62 \times 10^7 \pm 1.55 \times 10^7$  conidia/cm<sup>2</sup>, for mutant and wild-type strains, respectively;  $n = 3$  for each strain; mutant not shown in the graphs;  $P = 0.035$ ) in AMM culture medium. In the null *flpA* strain, however, the inhibition was statistically significant ( $1.86 \times 10^6 \pm 3.23 \times 10^5$  conidia/cm<sup>2</sup> in the null *flpA* strain,  $n = 3$ ,  $P = 0.003$ ) (Fig. 4A and D). The results obtained in the  $\Delta flbB$  background confirmed the trends described for the wild-type background, with the difference that both deletion or truncation of the last 45 codons completely inhibited conidia production, probably due to the additive effect on conidiation caused by the absence of *flbB* (26, 30, 40). However, the C-terminus of FlpA could play a minor role in these processes, as observed in the wild-type background.



**FIG 3** Evolutionary analysis of FlpA/AN10640, Stk47/AN8190, and FlpB/AN6312. Phylogenetic trees (maximum-likelihood method and the JTT matrix, with 50 replicates in each case) corresponding to the putative orthologs of FlpA (A), Stk47 (B) and FlpB (C) included in Table S3. Coverage (bar graphs in the trees) and score (shape plots) values for each hit compared to *A. nidulans* queries are included. The color key indicates which fungal class each ortholog belongs to.

(Continued on next page)

**FIG 3** (Continued)

(D) Predicted three-dimensional structures for FlpA, Stk47, and FlpB, modeled by Swiss-Model. The models cover the regions from His26 to Lys374 in FlpA, from Ser746 to His1052 in Stk47, and from Glu7 to Asn234 in FlpB, and are based on PDB structure 7jv7.1, which corresponds to the CTDK-1 complex of *S. pombe* and is shown in Fig. S2D (37). The alignments between FlpA, Stk47, or FlpB and the reference structure can be seen in Fig. S2A–C. (E) Predicted three-dimensional structure for a hypothetical complex formed by FlpA, Stk47, and FlpB, modeled by ColabFold. Full-length sequences of FlpA and FlpB were used, together with an N-terminally truncated form of Stk47 covering residues from Pro735 to Leu1067.

### Null mutants of *stk47* and *flpB* show the same phenotype as the null *flpA* strain

Since FlpA, Stk47, and FlpB may be the components of the CTDK-1 complex in *A. nidulans*, single-null mutants of *stk47* and *flpB* were also generated, and their phenotypes were compared to that of the  $\Delta flpA$  strain after 72 hours of culture at 37°C in solid AMM or AMM supplemented with 0.5 M  $\text{NaH}_2\text{PO}_4$  (Fig. 4E and F). Different combinations of double-null mutants were also generated by transformation of protoplasts of the single-null mutants with the corresponding deletion cassettes. The three single-null mutants showed a highly similar phenotype. We observed a slight increase in colony diameter and production of conidia only in the case of the null *flpB* strain. While the reference wild-type strain produced  $2.67 \times 10^7 \pm 0.82 \times 10^7$  conidia/cm<sup>2</sup>,  $\Delta flpA$ ,  $\Delta stk47$ , and  $\Delta flpB$  strains produced, respectively,  $5.94 \times 10^5 \pm 3.80 \times 10^5$ ,  $5.63 \times 10^5 \pm 2.11 \times 10^5$ , and  $1.02 \times 10^6 \pm 2.26 \times 10^5$  conidia/cm<sup>2</sup> ( $P = 0.032$  in the comparison between the wild-type and the null *flpA* strains,  $P = 0.908$  and  $0.172$  when  $\Delta flpA$  was compared to  $\Delta stk47$  and  $\Delta flpB$  strains,  $P = 0.063$  when null *stk47* and null *flpB* strains were compared;  $n = 3$  for each strain). Of note is the phenotypic difference between null *stk47* strains when *A. fumigatus pyrG* or *riboB* genes were used as selection markers (Fig. 4E and F). Conidia production increased from  $5.63 \times 10^5 \pm 2.11 \times 10^5$  conidia/cm<sup>2</sup> in the  $\Delta stk47::pyrG$  strain to  $1.38 \times 10^7 \pm 2.02 \times 10^6$  conidia/cm<sup>2</sup> in the  $\Delta stk47::riboB$  strain ( $P = 0.008$ ,  $n = 3$  for each strain).

Double-null mutants displayed a highly similar phenotype compared to their corresponding parental strains, and no additive effects in conidia production were observed after deletion of the second gene (Fig. 4E and F). The double-null  $\Delta flpA;\Delta flpB$  (generated after transformation of  $\Delta flpA$  protoplasts with the construct for *flpB* deletion) produced  $1.07 \times 10^6 \pm 2.75 \times 10^5$  conidia/cm<sup>2</sup> ( $P = 0.190$  compared to its parental strain,  $n = 3$  for each strain). Double-null mutants  $\Delta stk47;\Delta flpA$  and  $\Delta stk47;\Delta flpB$  (both generated by transformation of protoplast of the  $\Delta stk47::riboB$  strain) produced  $1.36 \times 10^7 \pm 2.04 \times 10^6$  and  $2.08 \times 10^7 \pm 1.34 \times 10^6$  conidia/cm<sup>2</sup> ( $P = 0.914$  and  $0.008$  when compared to their parental strain).

Finally, the ability to generate cleistothecia by the single-null *flpA*, *stk47*, and *flpB* mutants was assessed qualitatively. Figure 4G clearly shows that the mutants do not produce cleistothecia in our culture conditions (7 days of culture at 37°C in solid AMM). Overall, these results strongly suggest that FlpA, Stk47, and FlpB are necessary for both morphogenesis and sexual or asexual developmental processes. The phenotypic similarities among single-null and double-null mutants also suggest that the three proteins function in the same pathway, in correlation with their hypothetical participation in the formation of the CTDK-1 complex.

### $\Delta flpA$ , $\Delta stk47$ , and $\Delta flpB$ strains generate aberrant conidiophores with a deficient metula-to-phialide transition

The null *flbB* mutant fails to induce conidiophore development, while deletion of both *flpA* and *flbB* has an additive inhibitory effect on conidia production. Thus, we hypothesized that FlpA could have a role different from that carried out by FlbB. While the latter is necessary for the induction of asexual development, FlpA may play a role in the correct and timely generation of the cell types that form conidiophores (foot-cell, stalk, vesicle, metulae, phialides, and conidia) (13). To verify that, we carried out a phenotypic characterization of the  $\Delta flpA$  strain in submerged culture and under nitrogen

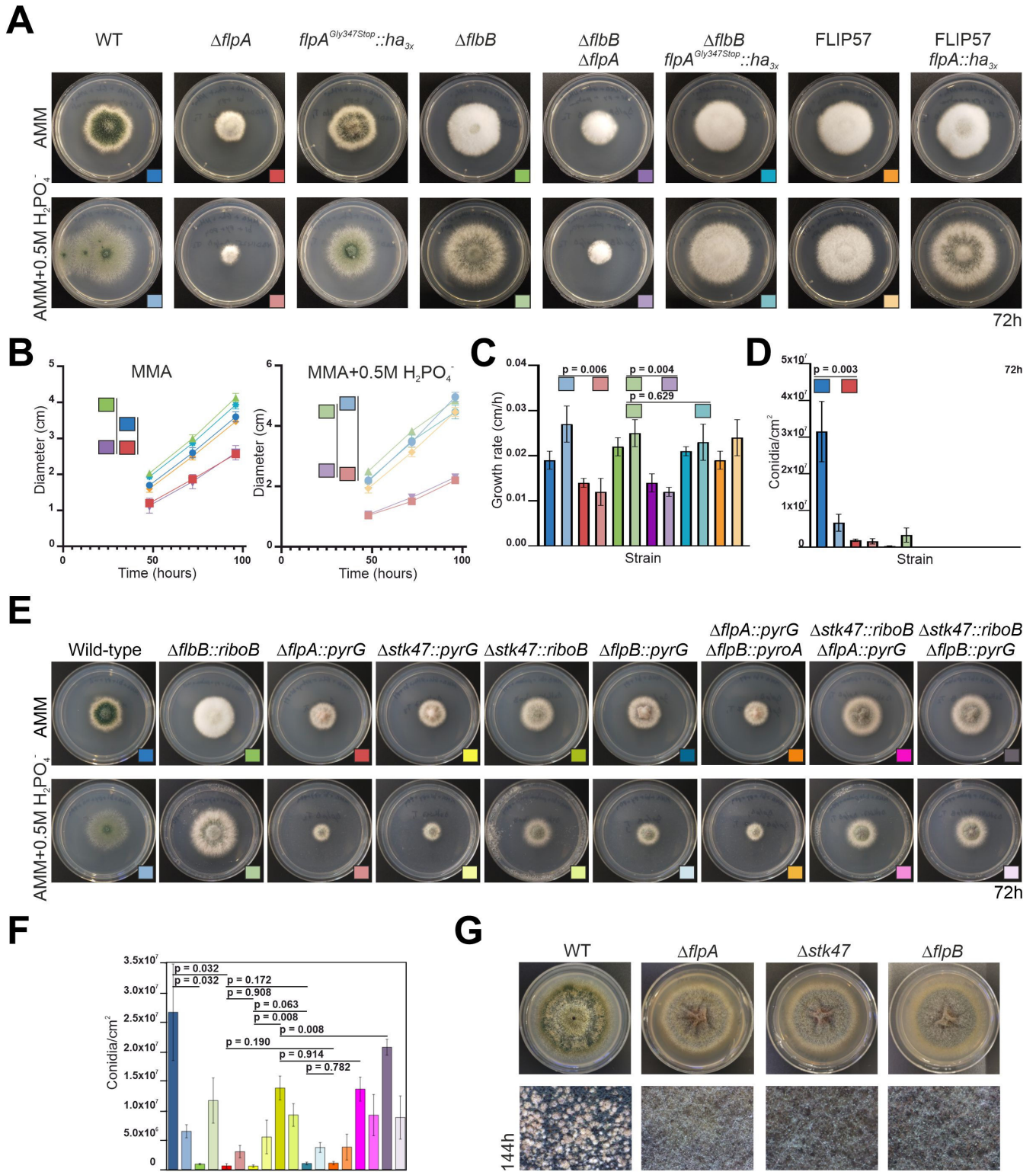


**FIG 4** Phenotypic analysis of  $\Delta flpA$ ,  $\Delta stk47$ , and  $\Delta flpB$  strains in solid media. (A) Phenotypes of parental (wild type,  $\Delta flbB$ , and FLIP57) and mutant strains  $\Delta flpA$  (wild-type and  $\Delta flbB$  genetic backgrounds),  $flpA^{Gly347Stop}::ha_{3x}$  (same two genetic backgrounds), and  $flpA::ha_{3x}$  (FLIP57 background), after 72 hours of culture at 37°C in AMM or AMM supplemented with 0.5 M  $NaH_2PO_4$ . Diameter of Petri plates is 5.5 cm. (B) Colony diameters for selected strains (see the color key in panel A) on AMM or AMM supplemented with 0.5 M  $NaH_2PO_4$  after 48, 72, and 96 hours of culture at 37°C. Each value is the mean of three replicates per strain and time point plus SD. (C) Radial growth rates for each of the strains analyzed in panel A. Each value is the average (plus SD) of the growth rates at (Continued on next page)

**FIG 4** (Continued)

the three time points analyzed. The values at each time point are based on three replicates per strain. (D) Conidia production (conidia/cm<sup>2</sup>) for each strain in panel A. Each value is the mean of three replicates plus SD. The values of *P* are shown where necessary in panels B–D. (E) Phenotypes of reference wild-type and  $\Delta flbB$  strains, together with those of single-null *flpA*, *stk47* (generated with *pyrG* or *riboB* markers), and *flpB* mutants, and double-null  $\Delta flpA::pyrG;\Delta flpB::pyrA$ ,  $\Delta stk47::riboB;\Delta flpA::pyrG$ , and  $\Delta stk47::riboB;\Delta flpB::pyrG$  mutants, after 72 hours of culture at 37°C in AMM or AMM supplemented with 0.5 M NaH<sub>2</sub>PO<sub>4</sub>. Diameter of Petri plates is 5.5 cm. (F) Quantification of conidia production (conidia/cm<sup>2</sup>) for the strains shown in panel E (see the color key in this panel). *P* values are included for specific comparisons (see main text). (G) Inhibition of cleistothecia production in  $\Delta flpA$ ,  $\Delta stk47$ , and  $\Delta flpB$  strains, compared to their parental wild-type strain, after 144 hours of culture at 37°C in AMM. Diameter of plates is 5.5 cm. Bottom magnifications correspond to the center of colonies. SD, standard deviation; WT, wild type; AMM and MMA, *Aspergillus* minimal medium.

starvation conditions (see Materials and Methods). As shown before, the wild-type strain produces mature conidiophores after 20 hours of culture at 37°C under nitrogen starvation conditions (Fig. 5A; upper block of images, left) (26, 41). The null *flbB* strain was not able to induce the production of conidiophores (Fig. 5A; upper block of images, second column). The  $\Delta flpA$  strain developed conidiophores and conidia under nitrogen starvation. Nevertheless, we repeatedly observed that, in those mutant conidiophores, metulae did not bud correctly into phialides (Fig. 5A; upper block of images, right; white arrowheads and magnifications) or that, in specific cases, secondary conidiophores emerged from aberrant primary conidiophores (Fig. 5A; lower block of images, column 2). Null *stk47* and *flpB* strains showed the same phenotype as the  $\Delta flpA$  strain (Fig. 5A; lower block of images, columns 3 and 4).

A hypothetical delay in spore germination was also assessed. Figure 5B shows that spores of the  $\Delta flpA$  mutant are delayed in germination compared to those of the reference wild-type strain. After 8 hours of incubation, 87.6 ± 0.5% of the wild-type spores had germinated, while only 59.3 ± 6.4% of the null *flpA* spores formed a germ tube (*n* = 2 replicates per strain), suggesting that there is a delay longer than 1 hour between the two strains.

Finally, distribution of septa in hyphae of the null strains of *flpA*, *stk47*, and *flpB* was analyzed and compared to that of the parental wild type (Fig. 5C). An altered pattern may explain the limited radial growth described previously. The calculated average distance among consecutive septa in wild-type hyphae was 65.6 ± 20.8 μm (*n* = 182 septa in 41 hyphae). Similar values were measured in the single-null strains, being 66.1 ± 26.1 μm, 65.0 ± 21.7 μm and 64.2 ± 21.5 μm in  $\Delta flpA$ ,  $\Delta flpB$ , and  $\Delta stk47$ , respectively (*n* = 97, 141, and 122 septa in 25, 29, and 35 hyphae; *P* > 0.05 in the three comparisons with the reference strain). Apparently, septa in the null strains were correctly distributed (not shown).

Overall, results explain the reduced *radii* of colonies and conidia yields described in the previous section and associate these phenotypic traits with a delayed germination but not an altered distribution of septa, at least in vegetative hyphae.

### FlpA, Stk47, and FlpB localize to nuclei in *A. nidulans* vegetative hyphae

If FlpA, Stk47, and FlpB form the CTDK-1 complex in *A. nidulans* and control the phosphorylation state of the C-terminus of the RNA polymerase II complex, they should localize to nuclei. We generated strains expressing a GFP-tagged version of each protein. When it was driven by the native promoter, FlpA fluorescence could not be detected (Fig. S3) and, consequently, a strain expressing a *gpdA<sub>p</sub><sup>mini</sup>*-driven (42) FlpA::GFP chimera was generated. FlpA::GFP was detected then in nuclei, probably in a cell cycle-dependent manner, since nuclear accumulation was lost during mitosis (Fig. 6A). Stk47::GFP and FlpB::GFP chimeras (driven by their native promoters) were also detected in nuclei of hyphae (Fig. 6B and C, respectively), confirming our initial hypothesis.

Karagiannis and Balasubramanian analyzed the nuclear localization of the *S. pombe* orthologs of FlpA and Stk47, Lsk1 (Ctk1) and Lsc1 (Ctk2) (43). The authors described that the nuclear localization of Lsc1/Ctk2 was lost in a null *lsc1/ctk1* background but that, in a null *lsc1/ctk2* background, Lsk1 remained at nuclei. We tested any interdependence

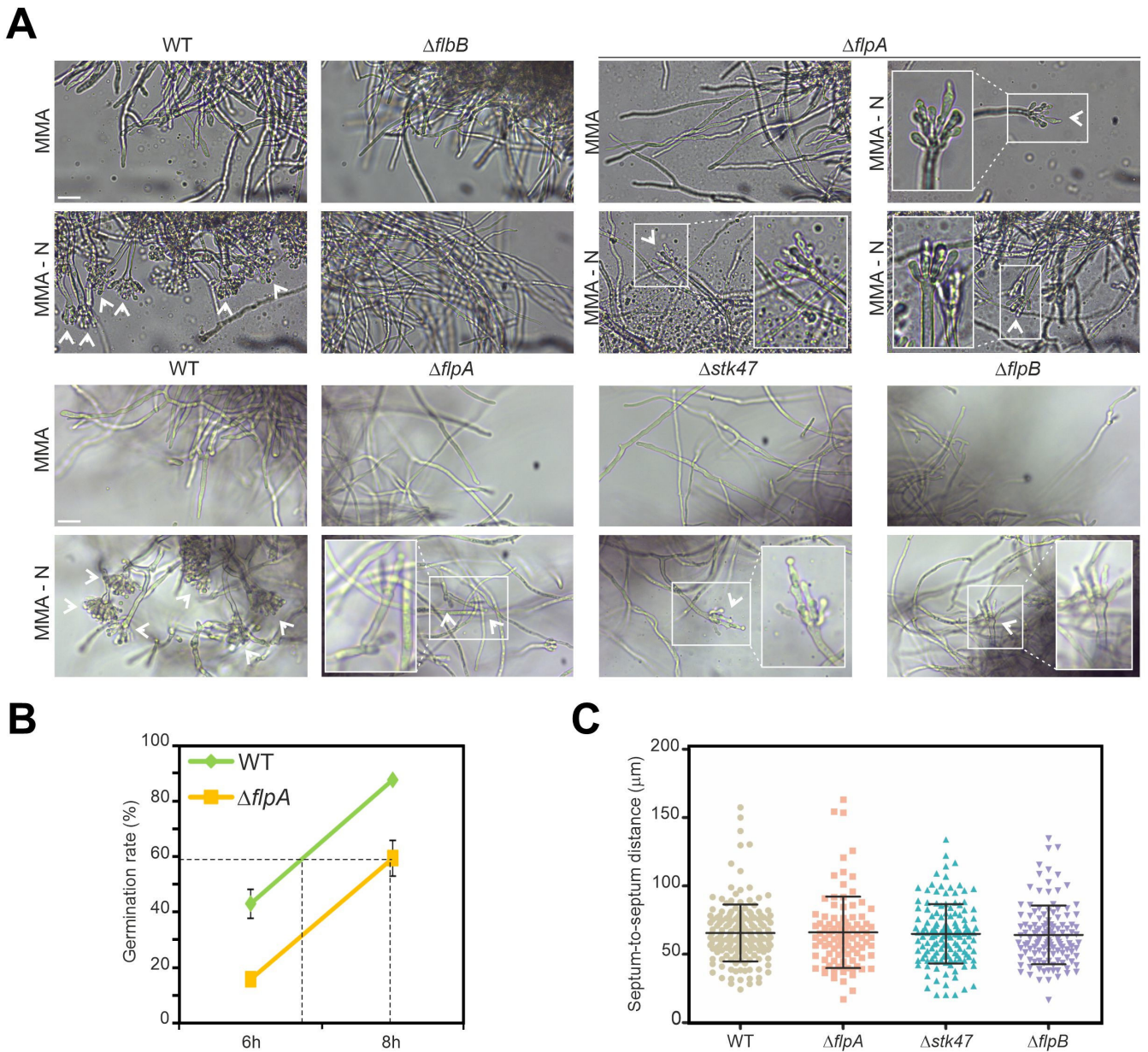


**FIG 5** Phenotypic characterization of  $\Delta flpA$ ,  $\Delta stk47$ , and  $\Delta flpB$  strains in liquid media. (A) (Top) Phenotype of the  $\Delta flpA$  strain in AMM (18 hours + 20 hours at 37°C and 200 rpm; row 1, column 3; see Materials and Methods) and under nitrogen starvation conditions (18-hour AMM + 20-hour AMM without a nitrogen source; row 2, columns 3 and 4), compared to the parental wild-type strain (column 1) and a  $\Delta flbB$  mutant (column 2). White arrowheads indicate the asexual structures generated by each strain. Those produced by the null  $flpA$  strain are zoomed to show that most metulae do not bud correctly into two phialides, rendering aberrant conidiophores. (Bottom) Phenotype of the reference wild-type strain and the mutants  $\Delta flpA$ ,  $\Delta stk47$ , and  $\Delta flpB$  under the same culture conditions as in the upper panel. (B) Percentages of wild-type and  $\Delta flpA$  conidia germinated in adequately supplemented AMM (37°C and 200 rpm), 6 and 8 hours after inoculation (see Materials and Methods). (C) Dot-plot showing septum-to-septum distances in null mutants  $\Delta flpA$ ,  $\Delta stk47$ , and  $\Delta flpB$  compared to the parental wild-type strain. Average and standard deviation values are included.  $P > 0.05$  in all comparisons with the wild type.

in nuclear localization for FlpA, Stk47, and FlpB with respect to the other potential interactors. With that aim, protoplasts of each single-null mutant were transformed with  $gpdA_p^{mini}::flpA::gfp$ ,  $stk47::gfp$  or  $flpB::gfp$  constructs, and the subcellular localization of the chimeras was analyzed (Fig. 6D through F, respectively). All chimeras accumulated in nuclei, with the exception of Stk47::GFP in a  $\Delta flpA$  background (Fig. 6E, left). These results suggest that the nuclear accumulation of Stk47 depends on FlpA but also that there are additional mechanisms enabling the nuclear import and accumulation of FlpA and FlpB.

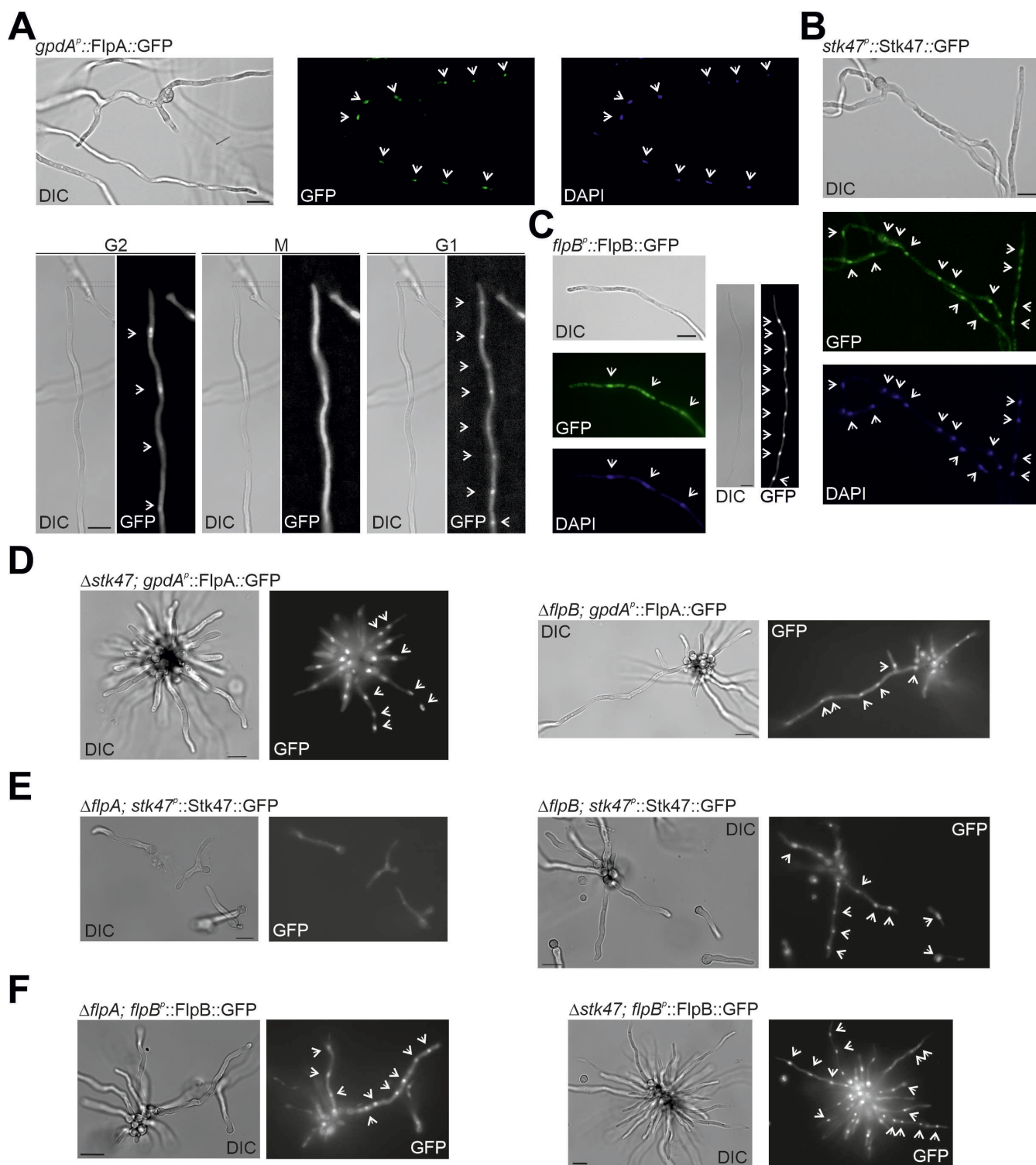


**FIG 6** FlpA, Stk47, and FlpB are located in nuclei of vegetative hyphae. Subcellular localization of (A) *gpdA<sup>Δ</sup>*-driven FlpA::GFP (see in Fig. S3 the analysis of the same chimera when it is driven by the native promoter), (B) Stk47::GFP, and (C) FlpB::GFP in vegetative hyphae of a wild-type strain. The nuclear localization of at least FlpA::GFP seems to be cell cycle dependent, as shown in panel A. DAPI (4',6-diamidino-2-phenylindole) was used as marker of nuclei in panels A–C. (D) Subcellular localization of *gpdA<sup>Δ</sup>*-driven FlpA::GFP in  $\Delta$ *stk47* and  $\Delta$ *flpB* backgrounds. (E) Subcellular localization of Stk47::GFP in  $\Delta$ *flpA* and  $\Delta$ *flpB* backgrounds. (F) Subcellular localization of FlpB::GFP in  $\Delta$ *flpA* and  $\Delta$ *stk47* backgrounds. Arrowheads highlight the position of nuclei. Scale bars = 10  $\mu$ m.

## The immunodetection-band pattern of Stk47 is altered in null *flpA/B* backgrounds

Next, we carried out immunodetection analyses to determine if the concentration and/or integrity of FlpA, Stk47, or FlpB are dependent on any of the other two activities. FlpA::GFP and FlpB::GFP showed, independently of the genetic background, bands at the expected sizes of 72 and 56 kDa, respectively (Fig. 7A). Due to the molecular weight of the Stk47::GFP chimera (155 kDa), we generated strains expressing the Stk47::HA<sub>3x</sub> chimera (128 kDa) in wild-type,  $\Delta flpA$ , and  $\Delta flpB$  genetic backgrounds. We detected two main pairs of bands at different molecular sizes (see red and green squares in Fig. 7B). The lightest band in the lower pair of bands (green square) was clearly more intense in  $\Delta flpA$  and  $\Delta flpB$  genetic backgrounds, while the heaviest pair of bands remained unaltered compared to the wild-type background. Despite the detection of these two main pairs of bands, we hypothesized that, considering their high molecular weight, they could hardly correspond to mono- or oligophosphorylation and that they rather corresponded to polyphosphorylation or to a different type of protein modification. Treatment with lambda phosphatase ( $\lambda$ PP; sodium orthovanadate was used as an inhibitor of phosphatase activity) did not alter the immunodetection pattern of Stk47::HA<sub>3x</sub> (Fig. 7C).

Although immunodetection experiments showed an altered Stk47::HA<sub>3x</sub> band pattern in the single-null mutants of *flpA* and *flpB*, they did not clarify if Stk47 is phosphorylated and if FlpA is the cyclin or one of the cyclins in charge of Stk47 phosphorylation. Thus, we carried out phosphopeptide enrichment analyses to compare the phosphoproteomes of single-null *flpA* and *stk47* strains with that of the wild-type strain (Table S2). Phosphopeptides corresponding to Stk47 were detected in the wild-type strain but not those corresponding to the large subunit of RNA pol II, Rpb1. The most notably affected function in the phosphoproteome of the  $\Delta flpA$  strain was that of serine/threonine-protein kinases, and this included the absence of phosphorylation of Stk47 (Fig. S4). However, results must be taken with care, due to a lack of reproducibility in the second replicate (see Discussion).

To analyze if FlpA and Stk47 form a protein complex, we carried out two types of pull-down assays. First, Stk47::HA<sub>3x</sub> or (*gpdA<sub>p</sub>*<sup>mini</sup>-driven) FlpA::HA<sub>3x</sub> chimeras were used as bait for HA-agarose resin (see Materials and Methods). Retained fractions were resolved in SDS-PAGE gels and analyzed through immunodetection. Despite the enrichment in each bait protein (Fig. S5), Liquid chromatography with tandem mass spectrometry (LC-MS/MS) analyses of those *R* fractions did not show significant enrichment in peptides corresponding to putative interactors (FlpA, Stk47, and FlpB) or any other *A. nidulans* cyclin and/or kinases (not shown). Thus, in a second approach, first, we incubated the GFP-trap resin with 3 mg of a crude protein extract of a strain expressing *gpdA<sub>p</sub>*<sup>mini</sup>-driven FlpA::GFP (bait; see Materials and Methods). In a second incubation, 3 mg of a crude protein extract of a strain expressing Stk47::HA<sub>3x</sub> was added. Fig. 7D shows that FlpA::GFP pulls down a fraction of Stk47::HA<sub>3x</sub>.

Then, an additional set of pull-down assays was carried out using the GFP-trap resin. In this case, FlpB::GFP was used as bait in the first incubation, while the second incubation was carried out with 3 mg of crude protein extracts of strains expressing *gpdA<sub>p</sub>*<sup>mini</sup>-driven FlpA::HA<sub>3x</sub> or Stk47::HA<sub>3x</sub>. Results in Fig. 7E show that FlpB::GFP pulls down both FlpA::HA<sub>3x</sub> and Stk47::HA<sub>3x</sub>, and that retention bands of Stk47::HA<sub>3x</sub> are not detected when FlpA activity is absent.

## Single-null mutants of *A. fumigatus* orthologs of *flpA*, *stk47*, and *flpB* show altered growth and developmental patterns

To analyze if FlpA, Stk47, and FlpB activities are also necessary for proper colony growth and developmental patterns in the genus *Aspergillus*, we generated single-null mutants of the three ortholog genes of *A. fumigatus*. Since this species is one of the main animal pathogens in the genus, we also analyzed if these activities are required for growth under stress conditions mimicking the host niche, for altered susceptibilities to

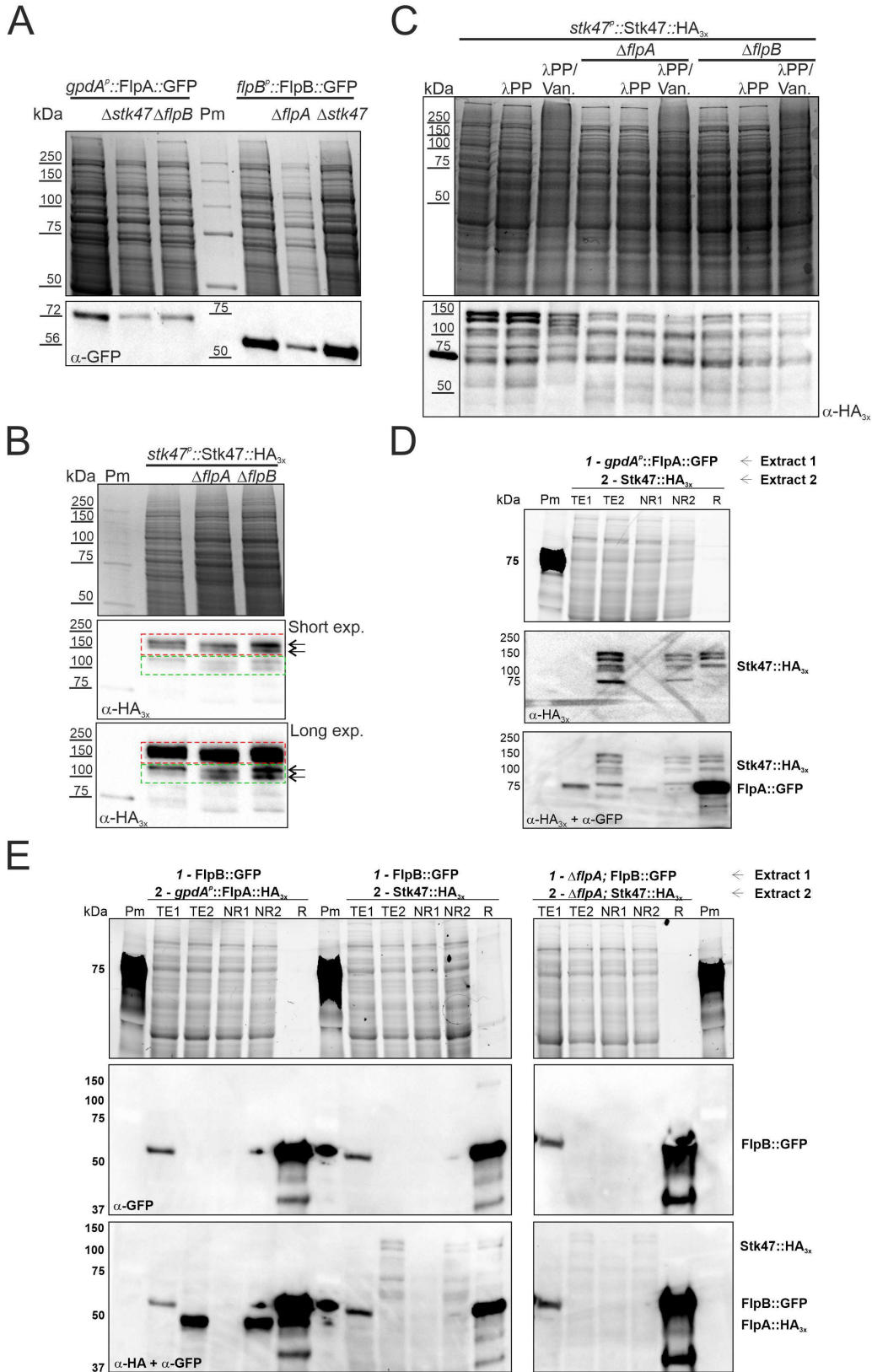


**FIG 7** Immunodetection of FlpA, Stk47, and FlpB. (A) Immunodetection of FlpA::GFP and FlpB::GFP chimeras, each in the parental wild-type background as well as null backgrounds of the other two genes. (B) Immunodetection of Stk47::HA<sub>3x</sub> in wild-type,  $\Delta$ *flpA*, and  $\Delta$ *flpB* genetic backgrounds. Stk47::HA<sub>3x</sub> shows pairs of bands (red and green squares). Note that within (Continued on next page)

**FIG 7** (Continued)

the green square, the lighter band increases its intensity in  $\Delta flpA$  and  $\Delta flpB$  backgrounds. (C) Treatment of crude protein extracts of Stk47::HA<sub>3x</sub> with  $\lambda$  phosphatase ( $\lambda$ PP) and  $\lambda$ PP plus sodium orthovanadate, the latter as an inhibitor of phosphatase activity. Gels stained with Bio-Safe Coomassie (Bio-Rad) are shown as loading controls in panels A–C. (D) Pull-down assay using the GFP-Trap resin of Chromotek. Resin samples were sequentially incubated (see Materials and Methods) with 3 mg of a crude protein extract of a strain expressing FlpA::GFP and after washing of the non-retained fraction, with 3 mg of a second crude protein extract of a strain expressing Stk47::HA<sub>3x</sub>. (E) Pull-down assays carried out by sequentially incubating the GFP-trap resin with 3 mg of a crude protein extract of a strain expressing FlpB::GFP (wild-type or  $\Delta flpA$  background), and then with 3 mg of a second crude protein extract of a strain expressing FlpA::HA<sub>3x</sub> or Stk47::HA<sub>3x</sub> (wild-type or  $\Delta flpA$  background). Strain-free gels (Bio-Rad) were used for protein electrophoresis in panels D and E. The image in row 1 was obtained as loading control before protein transference to polyvinylidene difluoride (PVDF) membranes. NR, non-retained; R, retained fraction; TE, total extract.

antifungal compounds and for virulence in a mouse model of invasive aspergillosis. The three single-null mutants showed a clear growth and developmental phenotype (Fig. 8A), with the difference that the radius of  $\Delta flpB$  colonies in medium supplemented with 0.5 M NaH<sub>2</sub>PO<sub>4</sub> is slightly bigger than those of  $\Delta flpA$  and  $\Delta stk47$  colonies (Fig. 8B). In all cases, the decrease in colony *radii* of single-null mutants compared with the reference wild-type strain was statistically significant ( $P < 0.05$  in the three comparisons). We also observed a delay in conidial germination in the three single-null mutants (Fig. 8C), which may partially explain the radial growth phenotypes described in Fig. 8A and B.

To test for impacts on growth in host-niche stress, we next examined the ability of the mutants to grow under oxidative, iron limitation, hypoxic, and cell wall stresses. All strains showed similar growth patterns in response to oxidative stress and under oxygen- or iron-limiting conditions (Fig. S6). However, we found that when  $\Delta stk47$ ,  $\Delta flpA$ , and  $\Delta flpB$  conidia were inoculated on medium supplemented with Congo red (CR) or calcofluor white (CFW), all mutants showed reduced radial growth compared to the reference wild-type strain (Fig. 8D). To confirm that the observed hypersusceptibility phenotype of the mutants to these cell wall stressors is not a result of a germination defect, we decided to test the ability of mature hyphae to develop under these conditions. Thus, we grew the same strains in minimal medium for 36 hours and transferred mycelial pellets of the same size to AMM agar plates supplemented with CR or CFW (80  $\mu$ g/mL). After 72 hours of culture, CR caused a  $48.48 \pm 5.01$  % growth reduction in the reference strain, when compared to minimal medium (Fig. 8E and F). Growth reduction was of  $64.34 \pm 4.33$  %,  $63.79 \pm 3.69$  %, and  $69.42 \pm 2.96$  % for  $\Delta stk47$ ,  $\Delta flpA$ , and  $\Delta flpB$  mutants, respectively ( $P < 0.05$  in all cases). The addition of CFW caused a  $28.66 \pm 4.33$  % growth reduction in the reference strain, while it was much greater in the single-null mutants, mainly in  $\Delta flpA$  ( $84.14 \pm 2.13$  %) and  $\Delta flpB$  ( $97.26 \pm 1.25$  %) ( $P < 0.05$  in all cases).

To see if this susceptibility would also be evident in response to cell wall-targeting antifungal drugs, we next tested susceptibility of the mutants to the echinocandin caspofungin, which inhibits  $\beta$ -glucan synthesis. Using a strip diffusion assay, we found the wild-type and  $\Delta flpA$  caspofungin minimum effective concentration (MEC) was 0.125  $\mu$ g/mL, and the  $\Delta flpB$  and  $\Delta stk47$  displayed a caspofungin MEC of 0.25  $\mu$ g/mL (Fig. S7). In addition, all strains displayed similar susceptibilities to membrane-targeting antifungals, with a voriconazole MIC ( range of 0.125–0.25  $\mu$ g/mL and posaconazole MIC of 0.25  $\mu$ g/mL. Therefore, loss of *stk47*, *flpB* or *flpA* does not impact antifungal susceptibility.

The hypersusceptibility of the three mutant strains to CR and CFW may suggest that the organization of the cell wall, and subsequently PAMP exposure, could be altered by deletion of *flpB*, *flpA*, or *stk47*. Altered PAMP exposure could subsequently lead to changes in host recognition during infection. To check if deletion of any gene alters host recognition, we next challenged THP-1 monocytes with conidia of the fungal strains and assayed inflammasome activation using interleukin (IL)-1 $\beta$  release as an endpoint (44). However, only a slightly lower release of IL-1 $\beta$  in the single-null mutants compared to

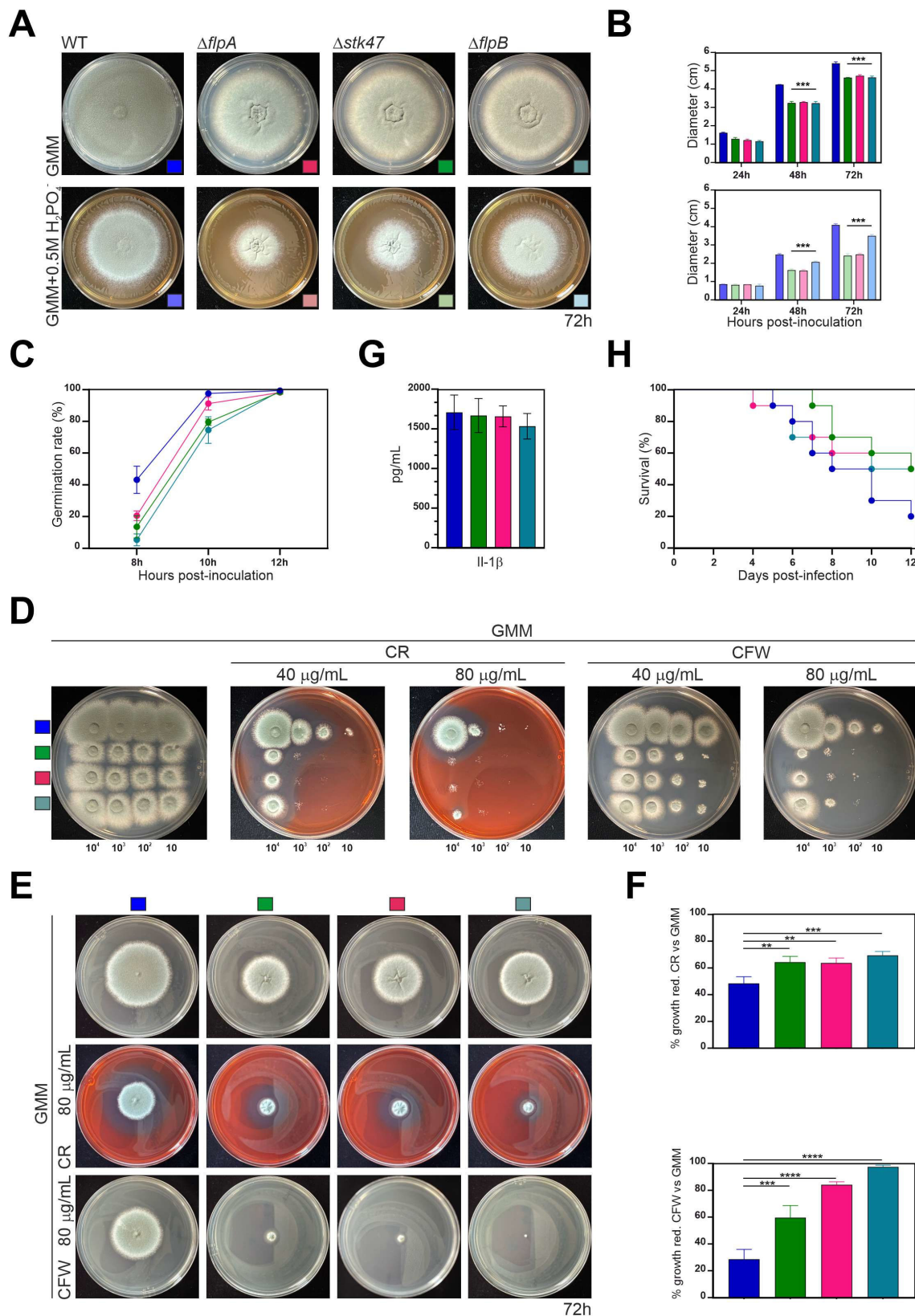


**FIG 8** Phenotype of single-null mutants of *flpA*, *stk47*, and *flpB* in *A. fumigatus*. (A) Phenotypes of wild-type and single-null *flpA*, *stk47*, and *flpB* strains of *A. fumigatus* after 72 hours of culture at 37°C in AMM or AMM supplemented with 0.5 M  $NaH_2PO_4$ . Diameter of plates is 5.5 cm. (B) Diameter of the colonies in panel A after 24, 48, and 72 hours of culture under the same conditions (\*\* $P < 0.01$ , compared to the reference  $\DeltaakuB$ - $pyrG^+$  strain;  $n = 3$  for each strain).

(Continued on next page)

**FIG 8** (Continued)

(C) Germination rate for each strain 8, 10, or 12 hours after inoculation ( $n = 3$  for each strain at each culture time). (D) Phenotypes of the strains after 48 hours of culture on AMM supplemented with 40 or 80  $\mu\text{g}/\text{mL}$  of CR or CFW. Conidia were inoculated at four different concentrations ( $10^4$ ,  $10^3$ ,  $10^2$ , or  $10^1$  conidia). Diameter of plates: 9 cm. (E) Phenotypes (72 hours at  $37^\circ\text{C}$ ) of the same strains after the transference of mycelial pellets grown in liquid minimal medium for 36 hours to plates containing minimal medium (control) or medium supplemented with 80  $\mu\text{g}/\text{mL}$  of CR or CFW. Pictures are representative of biological triplicates. (F) Bar graphs representing the percentage of growth reduction of each strain cultured in the presence of CR or CFW compared to minimal medium. Analysis was carried out by one-way analysis of variance with Dunnett's multiple comparison test. (Top)  $P \leq 0.0045$ ; (Bottom)  $P \leq 0.0006$ . (G) Quantification of release of interleukin-1 $\beta$  by THP-1 monocytes after co-culturing with conidia (multiplicity of infection: 10 conidia per THP-1 cell). (H) Percent survival of female CD-1 ( $n = 10$  mice per group) to infection by the wild-type or the *A. fumigatus* single-null mutants of *flpA*, *stk47*, and *flpB*. Survival was recorded daily, and the Kaplan-Meier curves were compared using log-rank tests in GraphPad Prism (v.9.2.0). CFW, calcofluor white; CR, Congo red. \*\*  $P < 0.01$ ; \*\*\*  $P < 0.001$ ; \*\*\*\*  $P < 0.0001$

the reference wild-type strain was detected, and these differences were not statistically significant ( $P > 0.05$  in the three comparisons; Fig. 8G). Therefore, we concluded that there are no significant differences in the ability of the mutants to trigger the inflammation.

Considering the growth, cell wall, and developmental phenotypes, we also analyzed the virulence of the *A. fumigatus* single-null mutants in a chemotherapeutic model of invasive aspergillosis. We observed that, after 12 days of infection, 50% of those animals challenged with the knockouts were alive, compared to only a 20% of mice infected with the parental strain. However, due to the limited sample size, the mortality rates between strains were not statistically significant (Fig. 8H). Taken together with the *in vitro* stress assay data, it is unlikely that *flpB*, *flpA*, or *stk47* play major roles in support of *A. fumigatus* virulence.

**DISCUSSION**

Among the different types of kinases, which are differentiated based on the sequence of the kinase domain, cyclin-dependent kinases, or CDKs, are serine/threonine kinases whose activity depends on the regulatory role carried out by a cyclin (45). Cyclins were named this way, first, because their protein levels fluctuated in a cyclical fashion during the cell cycle and, second, because they were defined by the presence of a cyclin box domain (see references within reference 46). Cyclins can be divided into two main groups, cell-cycle or canonical cyclins and transcriptional cyclins (46). The term transcriptional cyclins refers to their role in the regulation of RNA polymerase activity during transcription initiation and elongation. Thus, the role of cyclins goes beyond the control of events directly linked to the cell cycle. Furthermore, members of both groups of cyclins play cellular functions independently of a partner CDK. Similarly, CDKs also control transcription, metabolism, and cell differentiation (47).

Paolillo and coworkers identified, in the genomes of *A. nidulans* and *A. fumigatus*, 15 genes encoding cyclins that represent the three phylogenetic groups: group I or cell cycle cyclins (three in each genome), group II (seven in each genome), and group III (five in each genome), which mainly include transcriptional cyclins (34). On the other hand, De Souza and Osmani characterized the phenotypes of the single-null mutants of all the *A. nidulans* genes encoding kinases, totaling 128 (39). The null mutant of *AN8190/stk47* was described to show a strong growth defect and sensitivity to stress conditions triggered by sodium chloride. Our groups recently completed the systematic disruption of all putative protein kinase encoding genes in *A. fumigatus* (44). Interestingly, the *A. fumigatus* *stk47* disruption mutant displayed only wild-type phenotypes (our unpublished results), which is in contrast to the *A. fumigatus*  $\Delta$ *stk47* results reported here. However, the previously published work describing these results identified additional kinase disruption mutants that also displayed differential results upon disruption or deletion (44). These inconsistencies are presumed to be caused by continued transcriptional read through, and subsequent expression of truncated kinase mutants, in at least some of the disruption mutants contained within the *A. fumigatus* library. In the analysis of the set of *fluffy in phosphate* mutants of our *A. nidulans* collection, we identified a Gly347Stop substitution in *AN10640/flpA* as the mutation causing the FLIP57 phenotype.

Since FlpA is the ortholog of *S. pombe* cyclin Ctk2/Lsc1, its activity was linked to that of the CDK Stk47 and the hypothetical formation of an *A. nidulans* CTDK-1 complex (37, 43). In humans, CDK12-Cyclin K and CDK13-Cyclin K complexes would be the counterparts of the *S. pombe* Ctk1/Ctk2 complex (37). Nevertheless, the structure of the *S. pombe* CTDK-1 complex differs from the human counterparts in that it adds a third member, Ctk3, which is not conserved in *Homo sapiens*. Ctk3 enables the formation of the *S. pombe* CTDK-1 complex by interacting with both the cyclin and the kinase. This configuration may be conserved in the kingdom Fungi based on (i) the wide conservation patterns of the three components, (ii) the ColabFold prediction, (3) the highly similar phenotypes of the three single-null mutants in *A. nidulans* and *A. fumigatus*, and (4) the interaction patterns described in the pull-down assays carried out in this work.

The NLStradamus algorithm predicted the presence of a NLS sequence in AnStk47 (1,119 amino acids) but not in AnFlpA (392 amino acids) or AnFlpB (240 amino acids). However, our results showed that, in *A. nidulans*, nuclear accumulation of AnStk47 was dependent on AnFlpA activity, while nuclear accumulation of AnFlpA or AnFlpB was not dependent on AnStk47. This behavior is opposite to what was described in *S. pombe*. In fission yeast, Lsk1/Ctk1 was required for nuclear localization of Lsc1/Ctk2, but not inversely (43). Regarding the phosphorylation pattern of AnStk47, our results are not conclusive. The use of  $\lambda$  phosphatase did not modify the immunodetection-band pattern of AnStk47, and thus, we were not able to confirm that the Stk47 band pair altered in the  $\Delta flpA$  and  $\Delta flpB$  backgrounds corresponds to a (poly)phosphorylated form of the kinase. Previously, preliminary phosphopeptide-detection analyses by our group (unpublished) detected multiple phosphorylated peptides for AnStk47, suggesting that this kinase may be polyphosphorylated at Ser173, Ser177, Ser221, Ser498, Ser499, Ser505, Ser720, Thr1105, Ser1106, Ser1111, and Ser1112. In addition, the same analysis identified a phosphopeptide phosphorylated both at Ser2 and Ser5 of at least the heptad located at positions 1684–1690 (total length: 1745 aa) of the large subunit of RNA polymerase complex II, AnRpb1. Phosphopeptides for AnFlpA or AnFlpB were not detected. In the phosphopeptide-detection experiments carried out in this work, we were able to detect just a single phosphopeptide corresponding to the hypothetical phosphorylation of Ser720 of AnStk47 (no phosphopeptides for AnRpb1, AnFlpA, or AnFlpB were detected). Interestingly, this phosphopeptide was not detected in the null *flpA* strain, but, unfortunately, we have not been able to reproduce this result. Dephoure and colleagues described that the probability of observing site-determining ions is hampered by biases in peptide fragmentation that favor breakage at certain points and disfavor it at others (48). The same authors also stated that the type of protease used in sample processing (trypsin was used in this study; see Materials and Methods) may limit phosphorylation-site identification because not all phosphorylated residues are located in regions that will generate peptides detectable by mass spectrometry upon cleavage by a single protease (48). Future experiments will have to determine if FlpA is the cyclin or one of the cyclins for Stk47, if both proteins are required for phosphorylation of Rpb1, and if phosphorylation of Stk47 is a prerequisite for its nuclear import and/or retention.

Deletion of *flpA*, *stk47*, or *flpB* has pleiotropic effects on colony formation both in *A. nidulans* and *A. fumigatus*. Compared to the reference wild-type strain, (i) germination is delayed; (ii) the radius of the colony is decreased; (iii) aberrant conidiophores with a misscheduled transition from metulae to phialides are generated; and (iv) cleistothecia are not produced. If these three genes encode the components of the CTDK-1 complex, then these phenotypic traits are probably a consequence of an altered phosphorylation pattern of Rpb1. It has been described that phosphorylation of serine 2 of the C-terminal heptad repeats of Rpb1 is not an essential feature of general transcription in fission yeast but rather is critical for certain biological responses, such as sexual development (49). For example, Ser2 phosphorylation is critical during sexual differentiation of *S. pombe* for the induction of *ste11* transcription (49, 50), which encodes an HMG domain mating-type transcription factor. In correlation with these observations, the single-null mutants of *flpA*, *stk47* and *flpB* do not develop cleistothecia, in *A. nidulans*, in the conditions tested.

In the case of asexual development, the aberrant conidiophore structures described in this work are probably related to germination and growth defects, rather than (i) misscheduled or incomplete septation processes, as was described in *S. pombe* (43), or (ii) a direct role of these three proteins in the control of the expression patterns of UDA or CDP genes. The involvement of genes encoding regulators of germination and hyphal polarity in the formation of conidiophores has been previously described [see, e.g., the cases of *cdc42* and *rac1* orthologs of *A. nidulans* (51)].

The role of transcriptional cyclins and kinases in *A. nidulans* conidiation was previously described by the group of Fischer et al. (52, 53). PtkA, a Cdk9 kinase, interacts with cyclins PchA, PclA and PclB, and also with the kinase PipA, modulating its interaction partners and activity to control morphogenesis and development. Cdk9 is supposed to phosphorylate Ser2 residues in the CTD of Rpb1 and enable transcript elongation (54). Thus, the phosphorylation status of the CTD domain of the large subunit of RNA polymerase II is regulated by multiple cyclin-kinase complexes, which would modify their configuration, depending on the morphogenetic/developmental stage and the cell type. If confirmed in the future for FlpA and Stk47, such a mechanistic flexibility would enable, on the one hand, coordination of multiple pathways and accurate integration of the corresponding signals and, on the other hand, modification of the affinity of RNA polymerase II complex for target promoters.

## MATERIALS AND METHODS

### DNA sequencing

Genomic DNA of mutants FLIP57 and FLIP76 (Table S3) was extracted following standard procedures and using a phenol:chloroform:isoamyl alcohol mixture (25:24:1 vol/vol, PanReac AppliChem) (55). *An1459/pmtC* was amplified from these genomic samples using oligonucleotides PmtC-seq1 and PmtC-GSP2 and sequenced using oligonucleotides PmtC-seq1, PmtC-seq4, PmtC-Up, and PmtC-GSP2 (Table S4) to discard that the phenotypes of FLIP57 or FLIP76 were caused by mutations in *pmtC*, as occurred with FLIP166 (27). After integrity, purity and quantity checks (1.5% agarose electrophoresis and Qubit fluorimeter analyses), DNA samples were sequenced at Stabvida (Caparica, Portugal) using an Illumina Novaseq platform and 150-bp paired-end sequencing reads. The samples generated 16,607,684 (2,507 Mbp) and 16,279,736 sequence reads (2,458 Mbp), respectively, resulting in a theoretical average depth coverage of 83× and 82×, assuming a genome size of 30 Mbp.

### Bioinformatics

Reads were mapped using BWA-MEM (56) at the Galaxy platform (<https://usegalaxy.org/>), and the SAM files generated were converted to BAM counterparts (SAM-to-BAM). SNPs compared to the reference *A. nidulans* genome (*A\_nidulans\_FGSC\_A4\_version\_s10-m02-r03\_chromosomes.fasta*) were identified using Snippy. Results for strains FLIP57 and FLIP76 were compared also with those obtained for the mutant FLIP166 (27). Exonic mutations present in FLIP57 or FLIP76 but absent in the genomes of FLIP166 and the reference genome were selected as candidates. The Integrative Genomics Viewer software (57) was used to visualize and analyze DNA-seq and RNA-seq reads and to compare them with reference genomes.

Gene and protein sequence analyses were carried out in the FungiDB database (58). The presence of putative functional domains in protein sequences was predicted with InterPro (59), while the National Center for Biotechnology Information website (<https://blast.ncbi.nlm.nih.gov/Blast.cgi>) was used to BLAST query sequences. Clustal Omega was used to align protein sequences (60). The .msf file generated was used to visualize the alignments with Genedoc, and the clustal file generated was imported into MEGAX (61) in order to generate phylogenetic trees, which were edited using iTOL (62). Structure homology models for FlpA, Stk47, and FlpB were built with Swiss Model (63)

and ColabFold (64). The presence of nuclear localization signals was predicted using NLStradamus and SeqNLS algorithms (65, 66). Finally, GO analyses were carried out at the ShinyGO website (v.0.61) (67).

## Strains, oligonucleotides, and culture conditions

*Aspergillus nidulans* and *A. fumigatus* strains used in this study are listed in Table S3, while oligonucleotides can be seen in Table S4. Parental strains FLIP57 and FLIP76 were previously generated in a mutagenesis screening of a null *flbB* (BD177) strain (27). *A. nidulans* strains were cultivated in adequately supplemented liquid or solid AMM using glucose (2%) and ammonium tartrate (5 mM) as the sources of carbon and nitrogen, respectively (68, 69). A medium containing 25 g/L corn steep liquor (Sigma-Aldrich) and sucrose (0.09 M) as the carbon source was used as the fermentation medium (*Aspergillus* fermentation medium [AFM]) to culture samples for protein extraction (70). *A. fumigatus* strains were routinely cultured on AMM agar plates and  $\text{NaH}_2\text{PO}_4$  (0.5–0.65 M) was added to AMM to induce salt-stress conditions.

To assess sensitivity of *A. fumigatus* strains to CR or CFW, 10  $\mu\text{L}$  of 10-fold serial dilutions of conidia from each strain ( $10^4$ ,  $10^3$ ,  $10^2$ , and 10 conidia) were spotted on Petri plates filled with AMM supplemented with 40 or 80  $\mu\text{g}/\text{mL}$  of each compound (71). Plates were incubated for 48 and 72 hours at 37°C. Colony growth of the mutants was compared to that of the reference strain over the inoculum dilution range. To evaluate the susceptibility to CR and CFW using mature hyphae, 100 mL of AMM broth was inoculated with  $5 \times 10^7$  conidia and incubated for 36 hours at 37°C and 250 rpm. Then, mycelial pellets of each strain were isolated and placed on the center of Petri plates containing minimal medium supplemented with 80  $\mu\text{g}/\text{mL}$  of CR or CFW. Control plates contained no drug (minimal medium). The plates were incubated at 37°C and diameters were measured after 72 hours.

The ability of the *A. fumigatus* strains to respond to host-stress conditions was evaluated with the following assays: to determine the ability to grow in conditions of iron starvation,  $10^3$  conidia were point inoculated in the center of AMM plates or AMM lacking iron, and colony morphologies were observed after 48 hours at 37°C. To evaluate the growth in low oxygen environments, AMM plates containing  $10^3$  conidia of each strain were incubated in a hypoxia chamber at 37°C for 48 hours. The susceptibility to oxidative stress was evaluated as previously described (72), and growth inhibition halos were measured after 48 hours of incubation. Susceptibility of the strains to posaconazole, voriconazole, and caspofungin was determined using gradient diffusion strips (Liofilchem) in RPMI agar plates. Results were read after 24 or 48 hours of growth at 37°C. All the experiments were performed in biological triplicates.

The procedures developed by Tilburn and colleagues, or Szewczyk and colleagues, were used to obtain and transform protoplasts of *A. nidulans*, and select transformants on selective (lacking uridine and uracil, on the one hand, or pyridoxine, on the other hand) regeneration medium (regeneration minimal medium [RMM]: AMM supplemented with 1 M sucrose) (73, 74). Protoplasts of *A. fumigatus* strain  $\Delta\text{akuB-pyrG}^+$  were obtained and transformed using the procedure described by Yelton and colleagues (75). *AfflpA* (AFUB\_007390, *Afu1g07020*), *Afstk47* (AFUB\_051670; *Afu5g03160*), and *AfflpB* (AFUB\_027820, *Afu2g12130*) were deleted using a CRISPR-Cas9 gene editing procedure previously described by us (see below how DNA cassettes were generated) (76). Selection of transformants was carried out based on hygromycin resistance and correct integration of the DNA constructs was confirmed by diagnostic-PCR using the oligonucleotide pairs shown in Table S4. The control  $\Delta\text{akuB-pyrG}^+$  strain was constructed previously by replacing the mutant *pyrG* locus of the *A. fumigatus* KU80 $\Delta\text{pyrG}$  strain with the functional *A. parasiticus* *pyrG* homolog (71).

For fluorescence microscopy analyses, conidiospores of the strains of interest were incubated for approximately 18 hours at 25°C in Ibidi  $\mu$ -Dishes or Falcon multi-well plates containing, respectively, 2.0 or 1.5 mL of supplemented watch minimal medium (WMM) (77). Nuclei were visualized by adding to the cultures two drops of NucBlue™ live cell

stain readyProbes™ reagent (DAPI, Invitrogen) plus triton X100 (PanReac AppliChem, 0.05%) and by incubating 15–20 minutes at room temperature (RT) before fluorescence microscopy analysis.

To quantify conidia production in *A. nidulans*, asexual spores were point inoculated and cultured for 72 hours at 37°C. Conidia were collected in Tween 20 (0.02%), diluted (if necessary), and the total amount of conidia was determined using a Thoma cell counter. The number of conidia was divided by the area of the colony. Microsoft Excel was used to determine statistically significant differences in conidia production among strains and to draw the corresponding column bar graphs. Radii of *A. nidulans* colonies and their radial growth rates were determined by measuring and by comparing the diameter of the colonies after 48, 72, and 96 hours of culture in adequately supplemented AMM media.

Conidia of *A. fumigatus* were harvested from 5-day-old cultures grown on AMM. Colony morphologies of *A. fumigatus* mutants were assessed by spotting 5 µL containing 1,000 conidia onto the center of AMM plates (5.5 cm) and incubation for 72 hours at 37°C. Diameter of colonies were measured after 24, 48, and 72 hours of culture at 37°C.

The phenotypes of  $\Delta flpA$ ,  $\Delta stk47$ , and  $\Delta flpB$  mutants of *A. nidulans* under nitrogen starvation conditions were assessed as follows (25, 26, 41, 78). First,  $10^6$  conidia per mL of the mutants and their parental wild-type strain were inoculated in Erlenmeyer flasks filled with 25 mL of adequately supplemented liquid AMM. After 18 hours of culture at 37°C and 200 rpm, mycelia were filtered using Miracloth paper and inoculated in liquid AMM lacking a nitrogen source. After additional 20 hours of culture, phenotypes were analyzed using an Imaging Source DFK23UP031 digital camera coupled to a Nikon Eclipse E100 microscope.

Hypothetic germination defects of single-null mutants were assessed by inoculating  $5 \times 10^4$  (*A. nidulans*) conidia per mL in Erlenmeyer flasks filled with adequately supplemented liquid AMM, and by culturing them at 37°C and 200 rpm. For the evaluation of germination rates in *A. fumigatus*, 10,000 conidia from each strain were inoculated into AMM broth, poured over sterile coverslips, and incubated at 37°C in static conditions. After 6 or 8 (*A. nidulans*), or 8, 10, or 12 (*A. fumigatus*) hours of culture, the germinated conidia were counted from a minimum number of 100 conidia of each strain and time point. At least two replicates were analyzed per strain. The corresponding graphs were drawn with Microsoft Excel or GraphPad Prism (v.9.2.0).

Distribution of septa in *A. nidulans* hyphae was analyzed using fluorescence brightener 28 (CFW). Briefly, conidia of the strains of interest were inoculated in Falcon multi-well plates containing adequately supplemented WMM and incubated for approximately 18 hours at room temperature. Then, the culture medium was replaced by fresh WMM containing 0.01% CFW. Samples were incubated at room temperature for 5 minutes. Finally, the culture medium was replaced twice (plus additional 5 minutes of incubation) before observation using a Nikon Eclipse Ci manual upright microscope (see below; phase contrast and GFP images were processed). Septum-to-septum distances (a minimum of 90 for each strain in three biological replicates) were measured using ImageJ (<https://imagej.nih.gov/ij/>), and the corresponding scatter plot was generated using GraphPad Prism (v.5.01).

## Generation of DNA cassettes for transformation

The fusion-PCR technique was used to generate DNA constructs for transformation of *A. nidulans* protoplasts (79). For 3'-end gene tagging (wild-type or mutant versions), three DNA fragments were amplified and fused: first, 1.5 kb of the 3'-end of the coding region was amplified using oligonucleotides GSP1 and GSP2 (Table S4); second, *gfp*, *mCherry*, or *ha<sub>3x</sub>* tags plus the selection marker (*pyrG<sup>Afum</sup>* or *pyroA<sup>Afum</sup>* of *A. fumigatus*) were amplified using oligonucleotides GFP1 and GFP2 (2.6 or 1.9 kb, respectively, when *gfp::pyrG<sup>Afum</sup>*, *gfp::pyroA<sup>Afum</sup>*, or *mCherry::pyroA<sup>Afum</sup>*, and *ha<sub>3x</sub>::pyrG<sup>Afum</sup>* were amplified); third, 1.5 kb of the 3'-UTR region of the gene (oligonucleotides GSP3 and GSP4). The fusion-PCR reaction was carried out with an aliquot of each fragment and oligonucleotides GSP1 and GSP4.

To generate the constructs for *A. nidulans* gene deletion, the following three fragments were amplified and fused. First, 1.5 kb of the promoter region of the gene was amplified using oligonucleotides PP1 and PP2. Second, the selection markers *pyrG<sup>Afum</sup>* or *pyroA<sup>Afum</sup>* were amplified with oligonucleotides SMP1 and GFP2. Third, 1.5 kb of the 3'-UTR region of the gene was amplified with oligonucleotides GSP3 and GSP4. The fusion-PCR reaction was carried out with oligonucleotides PP1 and GSP4. To constitutively express FlpA::GFP or FlpA::HA<sub>3x</sub> chimeras under the control of the "mini" version of the promoter *gpdA<sup>P</sup>* (42), five fragments were amplified and fused (27, 80): first, 1.5 kb of the promoter using oligonucleotides PP1 and PP2'-ATG; second, the *gpdA<sup>P</sup>* promoter with oligonucleotides *gpdAUp* and *gpdADw*; third, the coding region of *flpA* was amplified with oligonucleotides *geneSP* and GSP2; fourth, the tag plus the selection marker (GFP1 and GFP2); and finally, 1.5 kb of the 3'-UTR region with oligonucleotides GSP3 and GSP4. The fusion of all those five fragments was done using oligonucleotides PP1 and GSP4. After transformation of *A. nidulans* protoplasts and genomic DNA extraction, correct recombination of the constructs was confirmed by diagnostic PCR using oligonucleotides sPP1 and sGSP4.

For *A. fumigatus* genetic engineering, hygromycin resistance repair templates, containing 40-bp micro-homology regions at both 5'- and 3'-ends of *Afstk47*, *AfflpA* or *AfflpB*, were amplified from plasmid pJMR2 (81) and utilized in a CRISPR/Cas9-mediated transformation to generate complete gene deletions (82).

### Analysis of cytokine release in THP-1 cells

Measurements of IL-1 $\beta$  released by THP-1 cells was carried out following procedures described previously (44, 83, 84). THP-1 cells were cultured in RPMI-1640 medium containing HEPES (25 mM) supplemented with heat-inactivated fetal bovine serum (10%), penicillin and streptomycin (100 U/mL), and 100  $\mu$ g/mL normocin, and assayed for viability by exclusionary trypan blue staining. Plating was carried out at a density of  $5 \times 10^4$  cells per well (96-well plates) in the same medium but lacking normocin. Phorbol 12-myristate 13-acetate at a final concentration of 100 nM was added, and cells were incubated for 24 hours to differentiate to a macrophage phenotype. Supernatants were discarded and replaced with 180  $\mu$ L of fresh RPMI (without phenol red) and 20  $\mu$ L of distilled water containing  $5 \times 10^5$  *A. fumigatus* conidia (multiplicity of infection, 10:1) of the single nulls or the reference strain. Cells were co-cultured for 16 hours at 37°C and 95% humidity. After incubation time, we collected the supernatants and measured the IL-1 $\beta$  concentrations using IL-1 $\beta$  enzyme-linked immunosorbent assay (ELISA) kits (Invitrogen) and following manufacturer instructions.

### Virulence assays in *A. fumigatus*

All animal experiments were carried out according to the protocols approved by the University of Tennessee Institutional Animal Care and Use Committee. Groups of 10, 6-week-old female CD-1 mice (Charles Rivers Laboratories) were immunosuppressed with 150 mg/kg of cyclophosphamide (neutropenic model) on day -3 and subsequently every third day starting again on day +1 (85) and an additional subcutaneous injection of triamcinolone acetonide on day -1. On the day of the infection, mice were slightly anesthetized with 3.5% isoflurane and inoculated intranasally with  $10^6$  freshly harvested conidia contained in 35  $\mu$ L of pyrogen-free saline solution. Mice were monitored at least twice a day and were given food and water *ad libitum*, and those animals showing severe signs of infection were humanely euthanized by anoxia with CO<sub>2</sub>. Mortality was monitored for 12 days. GraphPad Prism v.9.2.0 was used to plot survival data on a Kaplan-Meier curve and to carry out log-rank (Mantel-Cox) tests.

### Fluorescence microscopy

Subcellular localization of FlpA, Stk47, and FlpB was analyzed using a Zeiss Axio Observer Z1 inverted microscope as previously described (27, 86) or a Nikon Eclipse

Ci manual upright microscope. The former was equipped with a  $\times 63$  Plan Apochromat 1.4 oil immersion lens, and filters 38 (excitation at 470 nm and emission at 525 nm) and 43 (excitation at 545 nm and emission at 605 nm). The latter included 40 $\times$  and 100 $\times$  (oil) Nikon CFI Plan Fluor lenses, and Semrock filters DAPI-5060C (excitation at 377 nm and emission at 447 nm), GFP-4050B (excitation at 466 nm and emission at 525 nm), and mCherry-C (excitation at 562 nm and emission at 641 nm). ImageJ (<https://imagej.nih.gov/ij/>) (U.S. National Institutes of Health, Bethesda, MA, USA) was used to process fluorescence microscopy and phase contrast images.

### Protein extraction and immunodetection

For protein extraction, conidia of the strains of interest were collected in Tween 20 (4 mL, 0.02%) and washed twice by centrifugation at 4,000 rpm for 10 minutes. By default, inocula ( $10^6$  conidia/mL) were cultured in AFM (or AMM for phosphopeptide enrichment analyses) for 15 hours at 37°C and 200 rpm (87). Mycelia were filtered, frozen, lyophilized, homogenized, and resuspended in 1 mL per sample of A-40 buffer (25 mM HEPES, pH = 7.5, 50 mM KCl, 5 mM MgCl<sub>2</sub>, 0.1 M EDTA, 10% glycerol, and 0.5 mM dithiothreitol (DTT), supplemented with a protease inhibitor cocktail from Roche) or Trap buffer (10 mM HEPES, pH = 7.5, 1 mM EDTA, 0.1% NP-40, 150 mM NaCl, 0.5 mM DTT, plus a protease inhibitor cocktail from Roche; used in pull-down experiments with the GFP-Trap resin of Proteintech). After incubation at 4°C during 90 minutes with gentle end-over-end mixing, samples were centrifuged at 4°C and 13,000 rpm for 30 minutes. Supernatants were transferred to new 1.5 mL tubes, and protein concentrations were determined by the Bradford assay. Two hundred micrograms of protein was precipitated per sample with trichloroacetic acid (TCA) and purified with ethanol/ether 1:1 and 1:3 mixes, respectively. Finally, precipitates were resuspended in 80  $\mu$ L of SDS-PAGE loading buffer (62.5 mM Tris-HCl, pH = 6.8, 2% SDS, 5%  $\beta$ -mercaptoethanol, 6 M urea, and 0.05% bromophenol blue), and the integrity of the samples was assessed by polyacrylamide gel electrophoresis.

Alternatively, the procedure described by Hervás-Aguilar and Peñalva was followed (88). Mycelial samples (approximately 6 mg of lyophilized powder) were lysed using 1 mL of alkaline lysis buffer (0.2 M NaOH and 0.2%  $\beta$ -mercaptoethanol), and proteins were precipitated by adding 7.5% TCA. Samples were centrifuged and the supernatants were discarded, resuspending the pellets in 100  $\mu$ L Tris-base (1 M) and 200  $\mu$ L of SDS-PAGE loading buffer. Aliquots of 10  $\mu$ L were then loaded and separated in 10% polyacrylamide gels.

Samples of a hundred micrograms of protein from the crude extracts of the strains of interest were incubated with  $\lambda$ PP (total volume of 100  $\mu$ L per reaction; New England Biolabs) for 20 minutes at 30°C (89). Sodium orthovanadate (10 mM) was used as a  $\lambda$ PP inhibitor when necessary. After incubation, proteins were precipitated as described above and resuspended in 50  $\mu$ L of SDS-PAGE loading buffer. The integrity of samples was checked by polyacrylamide gel electrophoresis.

For immunodetection, protein samples were separated in Any kD Mini-PROTEAN TGX precast protein gels (Bio-Rad; stain-free gels were also used in specific experiments) before electro-transference (Trans-blot Turbo transfer system, Bio-Rad) to nitrocellulose filters. GFP- or HA<sub>3x</sub>-tagged proteins were detected using  $\alpha$ -GFP (1:1,000; Roche) or  $\alpha$ -HA<sub>3x</sub> (1:1,000; Santa Cruz Biotechnology) mouse monoclonal antibody cocktails. Peroxidase-conjugated  $\alpha$ -mouse (1:2,500; Jackson Immuno-Research Laboratories) was used as secondary antibody. Peroxidase activity was induced using the Clarity Western ECL substrate (Bio-Rad). Chemiluminescence was detected using a Chemidoc + XRS system (Bio-Rad).

### Phosphopeptide enrichment

Aliquots of approximately 300  $\mu$ g of the crude protein extracts were precipitated with acetone and resuspended in a mixture of urea (8 M) and ammonium bicarbonate

(50 mM). Proteins were reduced with dithiothreitol (10 mM) for 30 minutes at RT, alkylated with iodoacetamide (50 mM) in the dark for 30 minutes (RT), and digested with 15  $\mu$ g of trypsin overnight at 37°C. C18 SEP-PAK columns were used for desalting of peptide mixtures. Samples were dried at RT using a speedvac concentrator.

For TiO<sub>2</sub> phosphopeptide enrichment, slurry of Titansphere TiO (5  $\mu$ m) beads (cat. no.: 5020–75,000) was prepared in buffer C (300 mg/mL lactic acid; 53% acetonitrile, ACN; 0.07% trifluoroacetic acid, TFA) at 25 mg/mL.

Peptides pellets were resuspended in 600  $\mu$ L of buffer C, and 72  $\mu$ L of the titanium slurry was added to each sample. After incubation for 15–30 minutes at RT with end-over-end rotation, samples were centrifuged for spinning down the beads. Pellets were resuspended in 150  $\mu$ L of buffer C and transferred to top of the C8 disks stage tips (90). Buffer C was removed at moderate speed (10–30  $\mu$ L/min) using a syringe, and another 150  $\mu$ L of buffer C was added on top of the C8/TiO<sub>2</sub> stage tip and passed it through at the same speed for washing. Additional washing was carried out with 100  $\mu$ L of buffer B (80% ACN, 0.1% TFA) at the same conditions. For sample elution, 2  $\times$  50  $\mu$ L of buffer D (0.5% NH<sub>4</sub>OH) was applied, collecting each eluate in 100  $\mu$ L of TFA (2%). Samples were dried in a speedvac concentrator and reconstituted in TFA (0.1%) for desalting using C18 Zip-Tip columns.

For mass spectrometry analysis, fractions of 1/10 from each phosphopeptide-enriched sample were analyzed by nano-LC-MS/MS. Peptides were trapped onto a AcclaimPepMap 100 C18 (2 cm) precolumn (ThermoScientific), eluted onto a AcclaimPepMap 100 C18 column (inner diameter 75  $\mu$ m, 50 cm long, 2- $\mu$ m particle size; ThermoScientific) and separated using a 180-minute gradient (0%–21% buffer B for 60 minutes, 21%–35% buffer B for 100 minutes, 95% buffer B for 10 minutes, and 0% buffer B for 10 minutes; buffer A: 0.1% formic acid, 2% ACN; buffer B: 0.1% formic acid in ACN) at a flow-rate of 250 nL/min on a nanoEasy HPLC (Proxeon) coupled to a nanoelectrospray ion source (ThermoScientific).

A Q-Exactive mass spectrometer (ThermoScientific) in the positive ion mode was used for mass spectra acquisition. Full-scan MS spectra ( $m/z$  400–1,500) were acquired in the Orbitrap at a resolution of 70,000 at  $m/z$  200, and the 10 most intense ions were selected for tandem mass spectrometry (MS/MS). Fragmentation was carried out with a normalized collision energy of 27 eV. MS/MS scans were acquired with a starting mass of  $m/z$  200; automatic gain control (AGC) target was  $2e^5$ , resolution of 17,500 (at  $m/z$  200), intensity threshold of  $8e^3$ , isolation window of 2.0  $m/z$  units, and maximum IT was 100 ms. Charge state screening was enabled to reject unassigned, singly charged, and equal or more than seven protonated ions. A dynamic exclusion time of 20 seconds was used to discriminate against previously selected ions.

Mass spectra \*.raw files were searched against the *A. nidulans* fasta database (10,720 protein entries) using Sequest search engine through Proteome Discoverer (v.1.4.0.288, ThermoScientific). Search parameters included a maximum of two missed cleavages allowed, carbamidomethylation of Cys residues as a fixed modification and N-terminal acetylation, C-terminal oxidation, and Ser, Thr, and Tyr phosphorylation as variable modifications. Precursor and fragment mass tolerance was set to 10 ppm and 0.02 Da, respectively. Node 3 phosphoRS was used as scoring algorithm. This node evaluates statistical confidence of location of phosphorylation sites. Identified peptides were validated using Percolator algorithm with a  $q$ -value threshold of  $\leq 0.01$  (91).

## Pull-down assays

Pierce Anti-HA agarose beads (50  $\mu$ L per sample, ThermoScientific) were centrifuged 5–10 seconds at 12,000  $g$  and washed with a 1:1 vol of Tris buffered saline (TBS, ThermoScientific) by centrifugation at the same conditions. After discarding the liquid, 2 mg of crude protein lysate was added. Samples were incubated for 90 minutes at 4°C with gentle end-over-end mixing. After pelleting the resin with a 5- to 10-second pulse at 12,000  $g$ , supernatants were collected, and 200 mg of protein was precipitated with TCA. This fraction was saved for analysis of binding efficiency (non-retained, NR,

fraction). Then, the resin was washed thrice (pulses of 5–10 seconds at  $12,000 \times g$ ) with 500  $\mu\text{L}$  of TBS-T (TBS with 0.05% Tween 20). For elution of the bait protein, 1:1 ratios (vol/vol) of non-reducing 2 $\times$  SDS-PAGE loading buffer (20% glycerol, 4% SDS, 0.004% bromophenol blue, 12.5 mM Tris-HCl, pH = 6.8) were added before incubation for 10 minutes at 30°C. The resin was pelleted by centrifugation at  $12,000 \times g$  for 5–10 seconds, and the eluate was collected (retained fraction, *R*). Elution was repeated twice. Finally, a 1:1 vol of SDS-PAGE loading buffer was added to the resin, followed by incubation for 5 minutes at 95°C. Both NR and *R* fractions were resolved by SDS-PAGE electrophoresis and analyzed by immunodetection. *R* fractions were then analyzed by LC-MS/MS at CIC bioGUNE (Derio, Spain).

GFP-Trap beads (50  $\mu\text{L}$  per sample, Proteintech) were diluted in 500  $\mu\text{L}$  of dilution buffer (5 mM HEPES, pH = 7.5, 0.5 mM EDTA, 0.1% NP-40, 20 mM KCl, 150 mM NaCl, plus a protease inhibitor cocktail from Roche) and centrifuged for 2 minutes and  $2,500 \times g$  at 4°C. This washing step was repeated twice. Then, 3 mg of the crude protein extract containing the bait chimera (FlpA::GFP or FlpB::GFP) was added, and samples were incubated with gentle end-over-end mixing at 4°C for 90 minutes. Samples were centrifuged for 2 minutes and  $2,500 \times g$  at 4°C. The supernatants were collected and 200  $\mu\text{g}$  of this fraction was precipitated with TCA (fraction NR1). The resin was washed twice with 500  $\mu\text{L}$  of dilution buffer. Then, 3 mg of crude protein extracts containing the Stk47::HA<sub>3x</sub> or the FlpA::HA<sub>3x</sub> chimera was added, and the procedure was repeated (fraction NR2). Finally, 75  $\mu\text{L}$  of SDS-PAGE loading buffer was added; samples were incubated at 95°C for 5 minutes and centrifuged for 2 minutes and  $2,500 \times g$  at 4°C (fraction *R*). Both NR and *R* fractions were resolved by SDS-PAGE electrophoresis and analyzed by immunodetection.

## ACKNOWLEDGMENTS

Work at O.E.'s lab has been supported by Universidad del País Vasco (UPV)/Euskal Herriko Unibertsitatea (EHU) (GIU19/014) and the Basque Government (PIBA-PUE PIBA\_2020\_1\_0032; Elkartek KK-2021/43 and KK-2022/00107; and GIC IT1662-22). Work at CIB Margarita Salas-CSIC has been supported by Ministerio de Ciencia, Innovación y Universidades/Spanish Agencia Estatal de Investigación (RTI2018-094263-B-100, to E.A.E.). A.O. held a Margarita Salas grant (MARSA21/69), funded by Next-Generation EU, at the UPV/EHU. A.F. was a degree student with a collaboration grant by the Spanish Ministry of Education (21/19070). Z.A. was a master thesis student at O.E.'s lab, held an Ikertalent Fellowship funded by the Basque Government (PIF21/003) at the Basque Culinary Center, and is now a PhD student at O.E.'s lab with funds of the KK-2022/00107 project. Work at J.R.F.'s lab has been supported by National Institutes of Health grants R01-AI158442 and R01-AI143197. The funders had no role in study design, data collection and interpretation, or the decision to submit the work for publication.

We want to thank Dr. Ricardo Andrade, from the central microscopy services of the University of the Basque Country, for the assistance with their fluorescence microscope. The  $\Delta\text{stk47}::\text{riboB}$  strain of *A. nidulans* was generated by E. Requena, currently a PhD student at the Instituto Nacional de Investigación y Tecnología Agroalimentaria (Madrid, Spain).

Conceptualization: O.E., X.G., and E.A.E.; investigation: Z.A., A.O., A.F., X.G., A.M.-V., E.A.E., and O.E.; methodology: E.A.E., X.G., Z.A., and O.E.; supervision, E.A.E., X.G., and O.E.; writing—original draft: Z.A. and O.E.; review and editing: Z.A., A.O., A.F., X.G., A.M.-V., J.R.F., E.A.E., and O.E.

## AUTHOR AFFILIATIONS

<sup>1</sup>Laboratory of Biology, Department of Applied Chemistry, Faculty of Chemistry, University of the Basque Country, UPV/EHU, San Sebastian, Spain

<sup>2</sup>Department of Clinical Pharmacy and Translational Science, University of Tennessee Health Science Center, Memphis, Tennessee, USA

<sup>3</sup>Department of Cellular and Molecular Biology, Centro de Investigaciones Biológicas Margarita Salas (CSIC), Madrid, Spain

### AUTHOR ORCID*s*

Z. Agirrezabala  <http://orcid.org/0009-0007-2762-6360>  
 X. Guruceaga  <http://orcid.org/0000-0003-3258-2482>  
 A. Martin-Vicente  <http://orcid.org/0000-0003-0446-8906>  
 A. Otamendi  <http://orcid.org/0000-0002-1475-321X>  
 J. R. Fortwendel  <http://orcid.org/0000-0003-2301-4272>  
 E. A. Espeso  <http://orcid.org/0000-0002-5873-6059>  
 O. Etxebeste  <http://orcid.org/0000-0002-9786-6091>

### FUNDING

Funder	Grant(s)	Author(s)
<a href="#">Euskal Herriko Unibertsitatea (EHU)</a>	GIU19/014	O. Etxebeste
<a href="#">Eusko Jaurlaritza (Gobierno Vasco)</a>	PIBA_2020_1_0032	O. Etxebeste
<a href="#">Eusko Jaurlaritza (Gobierno Vasco)</a>	KK-2021/43	O. Etxebeste
<a href="#">Eusko Jaurlaritza (Gobierno Vasco)</a>	KK-2022/00107	O. Etxebeste
<a href="#">Eusko Jaurlaritza (Gobierno Vasco)</a>	IT1662-22	O. Etxebeste
<a href="#">MEC   Agencia Estatal de Investigación (AEI)</a>	RTI2018-094263-D-100	E. A. Espeso
<a href="#">HHS   National Institutes of Health (NIH)</a>	R01-AI158442	J. R. Fortwendel
<a href="#">HHS   National Institutes of Health (NIH)</a>	R01-AI143197	J. R. Fortwendel

### AUTHOR CONTRIBUTIONS

Z. Agirrezabala, Investigation, Methodology, Writing – original draft, Writing – review and editing | X. Guruceaga, Conceptualization, Investigation, Methodology, Supervision, Writing – review and editing | A. Martin-Vicente, Investigation, Writing – review and editing | A. Otamendi, Investigation, Writing – review and editing | A. Fagoaga, Investigation, Writing – review and editing | J. R. Fortwendel, Writing – review and editing | E. A. Espeso, Conceptualization, Investigation, Methodology, Supervision, Writing – review and editing | O. Etxebeste, Conceptualization, Investigation, Methodology, Supervision, Writing – original draft, Writing – review and editing

### ADDITIONAL FILES

The following material is available [online](#).

#### Supplemental Material

**File S1 (mBio02452-23-s0001.pdf).** Candidate exonic mutations found in FLIP57 and FLIP76.

**Supplemental figures (mBio02452-23-s0002.pdf).** Fig. S1 to S7.

**Supplemental legends (mBio02452-23-s0003.docx).** Legends for supplemental figures and tables.

**Table S1 (mBio02452-23-s0004.xlsx).** Probable FlpA, Stk47, and FlpB orthologs identified by BLAST analyses.

**Table S2 (mBio02452-23-s0005.xlsx).** List of phosphopeptides and phosphorylated proteins identified in crude protein extracts of the wild-type and the null flpA or null stk47 strains.

**Table S3 (mBio02452-23-s0006.docx).** Strains used in this work.

**Table S4 (mBio02452-23-s0007.docx).** Oligonucleotides used in this study.

## REFERENCES

- de Vries RP, Riley R, Wiebenga A, Aguilar-Osorio G, Amillis S, Uchima CA, Anderluh G, Asadollahi M, Askin M, Barry K, et al. 2017. Comparative genomics reveals high biological diversity and specific adaptations in the industrially and medically important fungal genus *Aspergillus*. *Genome Biol* 18:28. <https://doi.org/10.1186/s13059-017-1151-0>
- Latgé J-P, Chamilo G. 2019. *Aspergillus fumigatus* and aspergillosis in 2019. *Clin Microbiol Rev* 33:e00140-18. <https://doi.org/10.1128/CMR.00140-18>
- Meyer V, Andersen MR, Brakhage AA, Braus GH, Caddick MX, Cairns TC, de Vries RP, Haarmann T, Hansen K, Hertz-Fowler C, Krappmann S, Mortensen UH, Peñalva MA, Ram AFJ, Head RM. 2016. Current challenges of research on filamentous fungi in relation to human welfare and a sustainable bio-economy: a white paper. *Fungal Biol Biotechnol* 3:6. <https://doi.org/10.1186/s40694-016-0024-8>
- Meyer V, Basenko EY, Benz JP, Braus GH, Caddick MX, Csukai M, de Vries RP, Endy D, Frisvad JC, Gunde-Cimerman N, et al. 2020. Growing a circular economy with fungal biotechnology: a white paper. *Fungal Biol Biotechnol* 7:5. <https://doi.org/10.1186/s40694-020-00095-z>
- Ojeda-López M, Chen W, Eagle CE, Gutiérrez G, Jia WL, Swilaiman SS, Huang Z, Park H-S, Yu J-H, Cánovas D, Dyer PS. 2018. Evolution of asexual and sexual reproduction in the aspergilli. *Stud Mycol* 91:37–59. <https://doi.org/10.1016/j.simyco.2018.10.002>
- Todd RB, Davis MA, Hynes MJ. 2007. Genetic manipulation of *Aspergillus nidulans*: heterokaryons and diploids for dominance, complementation and haploidization analyses. *Nat Protoc* 2:822–830. <https://doi.org/10.1038/nprot.2007.113>
- Todd RB, Davis MA, Hynes MJ. 2007. Genetic manipulation of *Aspergillus nidulans*: meiotic progeny for genetic analysis and strain construction. *Nat Protoc* 2:811–821. <https://doi.org/10.1038/nprot.2007.112>
- Ugalde U, Rodríguez-Urra AB. 2014. The Mycelium Blueprint: insights into the cues that shape the filamentous fungal colony. *Appl Microbiol Biotechnol* 98:8809–8819. <https://doi.org/10.1007/s00253-014-6019-6>
- Etexbeste O, Otamendi A, Garzia A, Espeso EA, Cortese MS. 2019. Rewiring of transcriptional networks as a major event leading to the diversity of asexual multicellularity in fungi. *Crit Rev Microbiol* 45:548–563. <https://doi.org/10.1080/1040841X.2019.1630359>
- Etexbeste O, Espeso EA. 2020. *Aspergillus nidulans* in the post-genomic era: a top-model filamentous fungus for the study of signaling and homeostasis mechanisms. *Int Microbiol* 23:5–22. <https://doi.org/10.1007/s10123-019-00064-6>
- Ruger-Herreros C, Corrochano LM. 2020. Conidiation in *Neurospora crassa*: vegetative reproduction by a model fungus. *Int Microbiol* 23:97–105. <https://doi.org/10.1007/s10123-019-00085-1>
- Kirk P, Cannon P, Minter D, Stalpers J. 2008. Dictionary of the fungi. 10th ed. CAN International, Wallingford.
- Mims CW, Richardson EA, Timberlake WE. 1988. Ultrastructural analysis of conidiophore development in the fungus *Aspergillus nidulans* using freeze-substitution. *Protoplasma* 144:132–141. <https://doi.org/10.1007/BF01637246>
- Adams TH, Wieser JK, Yu J-H. 1998. Asexual sporulation in *Aspergillus nidulans*. *Microbiol Mol Biol Rev* 62:35–54. <https://doi.org/10.1128/MMBR.62.1.35-54.1998>
- Park H-S, Yu J-H. 2012. Genetic control of asexual sporulation in filamentous fungi. *Curr Opin Microbiol* 15:669–677. <https://doi.org/10.1016/j.mib.2012.09.006>
- Timberlake WE. 1980. Developmental gene regulation in *Aspergillus nidulans*. *Dev Biol* 78:497–510. [https://doi.org/10.1016/0012-1606\(80\)90349-8](https://doi.org/10.1016/0012-1606(80)90349-8)
- Park H-S, Lee M-K, Han K-H, Kim M-J, Yu J-H. 2019. Developmental decisions in *Aspergillus nidulans*, p 63–80. In Hoffmeister D, M Gressler (ed), *Biology of the fungal cell*. Springer International Publishing, Cham. <https://doi.org/10.1007/978-3-030-05448-9>
- Oiartzabal-Arango E, Perez-de-Nanclares-Arregi E, Espeso EA, Etexbeste O. 2016. Apical control of conidiation in *Aspergillus nidulans*. *Curr Genet* 62:371–377. <https://doi.org/10.1007/s00294-015-0556-0>
- Boylan MT, Mirabito PM, Willett CE, Zimmerman CR, Timberlake WE. 1987. Isolation and physical characterization of three essential conidiation genes from *Aspergillus nidulans*. *Mol Cell Biol* 7:3113–3118. <https://doi.org/10.1128/mcb.7.9.3113-3118.1987>
- Ni M, Yu J-H. 2007. A novel regulator couples sporogenesis and trehalose biogenesis in *Aspergillus nidulans*. *PLoS One* 2:e970. <https://doi.org/10.1371/journal.pone.0000970>
- Lee M-K, Kwon N-J, Choi JM, Lee I-S, Jung S, Yu J-H. 2014. NsdD is a key repressor of asexual development in *Aspergillus nidulans*. *Genetics* 197:159–173. <https://doi.org/10.1534/genetics.114.161430>
- Lee M-K, Kwon N-J, Lee I-S, Jung S, Kim S-C, Yu J-H. 2016. Negative regulation and developmental competence in *Aspergillus*. *Sci Rep* 6:28874. <https://doi.org/10.1038/srep28874>
- Oiartzabal-Arango E, Garzia A, Gorostidi A, Ugalde U, Espeso EA, Etexbeste O. 2015. Beyond asexual development: modifications in the gene expression profile caused by the absence of the *Aspergillus nidulans* transcription factor FibB. *Genetics* 199:1127–1142. <https://doi.org/10.1534/genetics.115.174342>
- Alkahyatt F, Ni M, Kim SC, Yu J-H, Harris S. 2015. The WOPR domain protein OsaA orchestrates development in *Aspergillus nidulans*. *PLoS One* 10:e0137554. <https://doi.org/10.1371/journal.pone.0137554>
- Etexbeste O, Herrero-García E, Araújo-Bazán L, Rodríguez-Urra AB, Garzia A, Ugalde U, Espeso EA. 2009. The bZIP-type transcription factor FibB regulates distinct morphogenetic stages of colony formation in *Aspergillus nidulans*. *Mol Microbiol* 73:775–789. <https://doi.org/10.1111/j.1365-2958.2009.06804.x>
- Etexbeste Oier, Herrero-García E, Cortese MS, Garzia A, Oiartzabal-Arango E, de los Ríos V, Ugalde U, Espeso EA. 2012. GmcA is a putative glucose-methanol-choline oxidoreductase required for the induction of asexual development in *Aspergillus nidulans*. *PLoS One* 7:e40292. <https://doi.org/10.1371/journal.pone.0040292>
- Otamendi A, Espeso EA, Etexbeste O. 2019. Identification and characterization of *Aspergillus nidulans* mutants impaired in asexual development under phosphate stress. *Cells* 8:1520. <https://doi.org/10.3390/cells8121520>
- Kriangkripiat T, Momany M. 2009. *Aspergillus nidulans* protein O-mannosyltransferases play roles in cell wall integrity and developmental patterning. *Eukaryot Cell* 8:1475–1485. <https://doi.org/10.1128/EC.00040-09>
- Picazo I, Etexbeste O, Requena E, Garzia A, Espeso EA. 2020. Defining the transcriptional responses of *Aspergillus nidulans* to cation/alkaline pH stress and the role of the transcription factor SitA. *Microb Genom* 6:mgen000415. <https://doi.org/10.1099/mgen.0.000415>
- Etexbeste O, Markina-Iñarriagaegui A, Garzia A, Herrero-García E, Ugalde U, Espeso EA. 2009. Kapl, a non-essential member of the Pse1P/Imp5 karyopherin family, controls colonial and asexual development in *Aspergillus nidulans*. *Microbiology (Reading)* 155:3934–3945. <https://doi.org/10.1099/mic.0.032615-0>
- Pantazopoulou A, Lemuh ND, Hatzinikolaou DG, Drevet C, Cecchetto G, Scazzocchio C, Diallinas G. 2007. Differential physiological and developmental expression of the UapA and AzgA purine transporters in *Aspergillus nidulans*. *Fungal Genet Biol* 44:627–640. <https://doi.org/10.1016/j.fgb.2006.10.003>
- Etexbeste O. 2021. Transcription factors in the fungus *Aspergillus nidulans*: markers of genetic innovation, network rewiring and conflict between genomics and transcriptomics. *J Fungi (Basel)* 7:600. <https://doi.org/10.3390/jof7080600>
- Garzia A, Etexbeste O, Rodríguez-Romero J, Fischer R, Espeso EA, Ugalde U. 2013. Transcriptional changes in the transition from vegetative cells to asexual development in the model fungus *Aspergillus nidulans*. *Eukaryot Cell* 12:311–321. <https://doi.org/10.1128/EC.00274-12>
- Paolillo V, Jenkinson CB, Horio T, Oakley BR. 2018. Cyclins in aspergilli: phylogenetic and functional analyses of group I cyclins. *Stud Mycol* 91:1–22. <https://doi.org/10.1016/j.simyco.2018.06.002>
- Nikolov DB, Chen H, Halay ED, Usheva AA, Hisatake K, Lee DK, Roeder RG, Burley SK. 1995. Crystal structure of a TFIIB–TBP–TATA-element ternary complex. *Nature* 377:119–128. <https://doi.org/10.1038/377119a0>
- Liu X, Marmorstein R. 2007. Structure of the retinoblastoma protein bound to adenovirus E1A reveals the molecular basis for viral oncoprotein inactivation of a tumor suppressor. *Genes Dev* 21:2711–2716. <https://doi.org/10.1101/gad.1590607>
- Xie Y, Lord CL, Clarke BP, Ivey AL, Hill PS, McDonald WH, Wente SR, Ren Y. 2021. Structure and activation mechanism of the yeast RNA Pol II CTD

- kinase CTDK-1 complex. *Proc Natl Acad Sci U S A* 118:e2019163118. <https://doi.org/10.1073/pnas.2019163118>
38. Rodrigues CH, Pires DE, Ascher DB. 2018. Dynamut: Predicting the impact of mutations on protein conformation, flexibility and stability. *Nucleic Acids Res* 46:W350–W355. <https://doi.org/10.1093/nar/gky300>
  39. De Souza CP, Hashmi SB, Osmani AH, Andrews P, Ringelberg CS, Dunlap JC, Osmani SA, Yu J-H. 2013. Functional analysis of the *Aspergillus nidulans* kinome. *PLoS One* 8:e58008. <https://doi.org/10.1371/journal.pone.0058008>
  40. Herrero-García E, Perez-de-Nanclares-Arregi E, Cortese MS, Markina-Iñarrairaegui A, Oñartzabal-Arango E, Etxebeste O, Ugalde U, Espeso EA. 2015. Tip-to-nucleus migration dynamics of the asexual development regulator FlbB in vegetative cells. *Mol Microbiol* 98:607–624. <https://doi.org/10.1111/mmi.13156>
  41. Skromne I, Sánchez O, Aguirre J. 1995. Starvation stress modulates the expression of the *Aspergillus nidulans* *brlA* regulatory gene. *Microbiology (Reading)* 141 (Pt 1):21–28. <https://doi.org/10.1099/00221287-141-1-21>
  42. Pantazopoulou A, Peñalva MA. 2009. Organization and dynamics of the *Aspergillus nidulans* golgi during apical extension and mitosis. *Mol Biol Cell* 20:4335–4347. <https://doi.org/10.1091/mbc.e09-03-0254>
  43. Karagiannis J, Balasubramanian MK. 2007. A cyclin-dependent kinase that promotes cytokinesis through modulating phosphorylation of the carboxy terminal domain of the RNA Pol II Rpb1P sub-unit. *PLoS One* 2:e433. <https://doi.org/10.1371/journal.pone.0000433>
  44. Souza ACO, Martín-Vicente A, Nywening AV, Ge W, Lowes DJ, Peters BM, Fortwendel JR. 2021. Loss of septation initiation network (SIN) kinases blocks tissue invasion and unlocks echinocandin cidal activity against *Aspergillus fumigatus*. *PLOS Pathog* 17:e1009806. <https://doi.org/10.1371/journal.ppat.1009806>
  45. Malumbres M. 2014. Cyclin-dependent kinases. *Genome Biol* 15:122. <https://doi.org/10.1186/gb4184>
  46. Quandt E, Ribeiro MPC, Clotet J. 2020. Atypical cyclins: the extended family portrait. *Cell Mol Life Sci* 77:231–242. <https://doi.org/10.1007/s00018-019-03262-7>
  47. Wood DJ, Endicott JA. 2018. Structural insights into the functional diversity of the CDK–cyclin family. *Open Biol* 8:180112. <https://doi.org/10.1098/rsob.180112>
  48. Dephoure N, Gould KL, Gygi SP, Kellogg DR. 2013. Mapping and analysis of phosphorylation sites: a quick guide for cell biologists. *Mol Biol Cell* 24:535–542. <https://doi.org/10.1091/mbc.E12-09-0677>
  49. Coudreuse D, van Bakel H, Dewez M, Soutourina J, Parnell T, Vandenhoute J, Cairns B, Werner M, Hermand D. 2010. A gene-specific requirement of RNA polymerase II CTD phosphorylation for sexual differentiation in *S. pombe*. *Curr Biol* 20:1053–1064. <https://doi.org/10.1016/j.cub.2010.04.054>
  50. Sukegawa Y, Yamashita A, Yamamoto M. 2011. The fission yeast stress-responsive MAPK pathway promotes meiosis via the phosphorylation of Pol II CTD in response to environmental and feedback cues. *PLoS Genet* 7:e1002387. <https://doi.org/10.1371/journal.pgen.1002387>
  51. Virag A, Lee MP, Si H, Harris SD. 2007. Regulation of hyphal morphogenesis by *cdc42* and *rac1* homologues in *Aspergillus nidulans*. *Mol Microbiol* 66:1579–1596. <https://doi.org/10.1111/j.1365-2958.2007.06021.x>
  52. Bathe F, Kempf C, Osmani SA, Osmani AH, Hettlinger S, Wohlmann E, Fischer R. 2010. Functional characterization of a new member of the *cdk9* family in *Aspergillus nidulans*. *Eukaryot Cell* 9:1901–1912. <https://doi.org/10.1128/EC.00384-09>
  53. Kempf C, Bathe F, Fischer R. 2013. Evidence that two Pcl-like cyclins control *cdk9* activity during cell differentiation in *Aspergillus nidulans* asexual development. *Eukaryot Cell* 12:23–36. <https://doi.org/10.1128/EC.00181-12>
  54. Anshabo AT, Milne R, Wang S, Albrecht H. 2021. Cdk9: a comprehensive review of its biology, and its role as a potential target for anti-cancer agents. *Front Oncol* 11:678559. <https://doi.org/10.3389/fonc.2021.678559>
  55. Garzia A, Etxebeste O, Herrero-García E, Fischer R, Espeso EA, Ugalde U. 2009. *Aspergillus nidulans* FlbE is an upstream developmental activator of conidiation functionally associated with the putative transcription factor FlbB. *Mol Microbiol* 71:172–184. <https://doi.org/10.1111/j.1365-2958.2008.06520.x>
  56. Li H. 2013. Aligning sequence reads, clone sequences and assembly contigs with BWA-MEM.
  57. Robinson JT, Thorvaldsdóttir H, Winckler W, Guttman M, Lander ES, Getz G, Mesirov JP. 2011. Integrative genomics viewer. *Nat Biotechnol* 29:24–26. <https://doi.org/10.1038/nbt.1754>
  58. Basenko E, Pulman J, Shanmugasundram A, Harb O, Crouch K, Starns D, Warrenfeltz S, Aurrecochea C, Stoeckert C, Kissinger J, Roos D, Hertz-Fowler C. 2018. Fungidb: an integrated bioinformatic resource for fungi and oomycetes. *JoF* 4:39. <https://doi.org/10.3390/jof4010039>
  59. Hnatiuk MJ, Noss R, Mitchell AL, Matthews AL. 2019. The current state of genetic counseling assistants in the United States. *J Genet Couns* 28:962–973. <https://doi.org/10.1002/jgc4.1148>
  60. Sievers F, Wilm A, Dineen D, Gibson TJ, Karplus K, Li W, Lopez R, McWilliam H, Remmert M, Söding J, Thompson JD, Higgins DG. 2011. Fast, scalable generation of high-quality protein multiple sequence alignments using clustal omega. *Mol Syst Biol* 7:539. <https://doi.org/10.1038/msb.2011.75>
  61. Kumar S, Stecher G, Li M, Niyaz C, Tamura K. 2018. MEGA X: molecular evolutionary genetics analysis across computing platforms. *Mol Biol Evol* 35:1547–1549. <https://doi.org/10.1093/molbev/msy096>
  62. Letunic I, Bork P. 2019. Interactive tree of life (iTOL) V4: recent updates and new developments. *Nucleic Acids Res* 47:W256–W259. <https://doi.org/10.1093/nar/gkz239>
  63. Waterhouse A, Bertoni M, Bienert S, Studer G, Tauriello G, Gumienny R, Heer FT, de Beer TAP, Rempfer C, Bordoli L, Lepore R, Schwede T. 2018. SWISS-MODEL: homology modelling of protein structures and complexes. *Nucleic Acids Res* 46:W296–W303. <https://doi.org/10.1093/nar/gky427>
  64. Mirdita M, Schütze K, Moriwaki Y, Heo L, Ovchinnikov S, Steinegger M. 2022. Colabfold - making protein folding accessible to all. *Nat Methods* 19:679–682. <https://doi.org/10.1038/s41592-022-01488-1>
  65. Nguyen Ba AN, Pogoutse A, Provart N, Moses AM. 2009. NLStradamus: a simple hidden markov model for nuclear localization signal prediction. *BMC Bioinformatics* 10:202. <https://doi.org/10.1186/1471-2105-10-202>
  66. Lin J, Hu J, Dalby AR. 2013. SeqNLS: nuclear localization signal prediction based on frequent pattern mining and linear motif scoring. *PLoS ONE* 8:e76864. <https://doi.org/10.1371/journal.pone.0076864>
  67. Ge SX, Jung D, Yao R, Valencia A. 2020. ShinyGO: a graphical gene-set enrichment tool for animals and plants. *Bioinformatics* 36:2628–2629. <https://doi.org/10.1093/bioinformatics/btz931>
  68. Cove DJ. 1966. The induction and repression of nitrate reductase in the fungus *Aspergillus nidulans*. *Biochimica et Biophysica Acta (BBA) - Enzymol Biological Oxidation* 113:51–56. [https://doi.org/10.1016/S0926-6593\(66\)80120-0](https://doi.org/10.1016/S0926-6593(66)80120-0)
  69. Käfer E. 1965. Origins of translocations in *Aspergillus nidulans*. *Genetics* 52:217–232. <https://doi.org/10.1093/genetics/52.1.217>
  70. Galindo A, Calcagno-Pizarelli AM, Arst HN, Peñalva MÁ. 2012. An ordered pathway for the assembly of fungal ESCRT-containing ambient pH signalling complexes at the plasma membrane. *J Cell Sci* 125:1784–1795. <https://doi.org/10.1242/jcs.098897>
  71. Al Abdallah Q, Martín-Vicente A, Souza ACO, Ge W, Fortwendel JR. 2018. C-terminus proteolysis and palmitoylation cooperate for optimal plasma membrane localization of rasi in *Aspergillus fumigatus*. *Front. Microbiol* 9. <https://doi.org/10.3389/fmicb.2018.00562>
  72. Martín-Vicente A, Souza ACO, Nywening AV, Ge W, Fortwendel JR. 2020. Overexpression of the *Aspergillus fumigatus* small GTPase, RsrA, promotes polarity establishment during germination. *JoF* 6:285. <https://doi.org/10.3390/jof6040285>
  73. Tilburn J, Sczaccocchio C, Taylor GG, Zabicky-Zissman JH, Lockington RA, Davies RW. 1983. Transformation by integration in *Aspergillus nidulans*. *Gene* 26:205–221. [https://doi.org/10.1016/0378-1119\(83\)90191-9](https://doi.org/10.1016/0378-1119(83)90191-9)
  74. Szewczyk E, Nayak T, Oakley CE, Edgerton H, Xiong Y, Taheri-Talesh N, Osmani SA, Oakley BR. 2006. Fusion PCR and gene targeting in *Aspergillus nidulans*. *Nat Protoc* 1:3111–3120. <https://doi.org/10.1038/nprot.2006.405>
  75. Yelton MM, Hamer JE, Timberlake WE. 1984. Transformation of *Aspergillus nidulans* by using a *trpC* plasmid. *Proc Natl Acad Sci U S A* 81:1470–1474. <https://doi.org/10.1073/pnas.81.5.1470>
  76. Al Abdallah Q, Souza ACO, Martín-Vicente A, Ge W, Fortwendel JR. 2018. Whole-genome sequencing reveals highly specific gene targeting by *In vitro* assembled *cas9*-ribonucleoprotein complexes in *Aspergillus fumigatus*. *Fungal Biol Biotechnol* 5:11. <https://doi.org/10.1186/s40694-018-0057-2>

77. Peñalva MA. 2005. Tracing the endocytic pathway of *Aspergillus nidulans* with Fm4-64. *Fungal Genet Biol* 42:963–975. <https://doi.org/10.1016/j.fgb.2005.09.004>
78. Etxebeste O, Ni M, Garzia A, Kwon NJ, Fischer R, Yu JH, Espeso EA, Ugalde U. 2008. Basic-zipper-type transcription factor FlbB controls asexual development in *Aspergillus nidulans*. *Eukaryot Cell* 7:38–48. <https://doi.org/10.1128/EC.00207-07>
79. Yang L, Ukil L, Osmani A, Nahm F, Davies J, De Souza CPC, Dou X, Perez-Balaguer A, Osmani SA. 2004. Rapid production of gene replacement constructs and generation of a green fluorescent protein-tagged centromeric marker in *Aspergillus nidulans*. *Eukaryot Cell* 3:1359–1362. <https://doi.org/10.1128/EC.3.5.1359-1362.2004>
80. Otamendi A, Perez-de-Nanclares-Arregi E, Oiartzabal-Arano E, Cortese MS, Espeso EA, Etxebeste O. 2019. Developmental regulators FlbE/D orchestrate the polarity site-to-nucleus dynamics of the fungal bZIP transcription factor FlbB. *Cell Mol Life Sci* 76:4369–4390. <https://doi.org/10.1007/s00018-019-03121-5>
81. Rybak JM, Ge W, Wiederhold NP, Parker JE, Kelly SL, Rogers PD, Fortwendel JR. 2019. Mutations in *hmg1*, challenging the paradigm of clinical triazole resistance in *Aspergillus fumigatus*. *mBio* 10:e00437-19. <https://doi.org/10.1128/mBio.00437-19>
82. Al Abdallah Q, Ge W, Fortwendel JR, Mitchell AP. 2017. A simple and universal system for gene manipulation in *Aspergillus fumigatus*: *In vitro*-assembled cas9-guide RNA ribonucleoproteins coupled with microhomology repair templates. *mSphere* 2. <https://doi.org/10.1128/mSphere.00446-17>
83. Willems HME, Lowes DJ, Barker KS, Palmer GE, Peters BM. 2018. Comparative analysis of the capacity of the *Candida* species to elicit vaginal immunopathology. *Infect Immun* 86:e00527-18. <https://doi.org/10.1128/IAI.00527-18>
84. Saïd-Sadier N, Padilla E, Langsley G, Ojcius DM. 2010. *Aspergillus fumigatus* stimulates the NLRP3 inflammasome through a pathway requiring ROS production and the Syk tyrosine kinase. *PLoS One* 5:e10008. <https://doi.org/10.1371/journal.pone.0010008>
85. Souza ACO, Al Abdallah Q, DeJarnette K, Martin-Vicente A, Nywening AV, DeJarnette C, Sansevere EA, Ge W, Palmer GE, Fortwendel JR. 2019. Differential requirements of protein geranylgeranylation for the virulence of human pathogenic fungi. *Virulence* 10:511–526. <https://doi.org/10.1080/21505594.2019.1620063>
86. Perez-de-Nanclares-Arregi E, Etxebeste O. 2014. Photo-convertible tagging for localization and dynamic analyses of low-expression proteins in filamentous fungi. *Fungal Genet Biol* 70:33–41. <https://doi.org/10.1016/j.fgb.2014.06.006>
87. Fernández-Martínez J, Brown CV, Díez E, Tilburn J, Arst HN Jr, Peñalva MA, Espeso EA. 2003. Overlap of nuclear localisation signal and specific DNA-binding residues within the zinc finger domain of PacC. *J Mol Biol* 334:667–684. <https://doi.org/10.1016/j.jmb.2003.09.072>
88. Hervás-Aguilar A, Peñalva MA. 2010. Endocytic machinery protein SlaB is dispensable for polarity establishment but necessary for polarity maintenance in hyphal tip cells of *Aspergillus nidulans*. *Eukaryot Cell* 9:1504–1518. <https://doi.org/10.1128/EC.00119-10>
89. Hernández-Ortiz P, Espeso EA. 2013. Phospho-regulation and nucleocytoplasmic trafficking of CrzA in response to calcium and alkaline-pH stress in *Aspergillus nidulans*. *Mol Microbiol* 89:532–551. <https://doi.org/10.1111/mmi.12294>
90. Rappsilber J, Mann M, Ishihama Y. 2007. Protocol for micro-purification, enrichment, pre-fractionation and storage of peptides for proteomics using stagetips. *Nat Protoc* 2:1896–1906. <https://doi.org/10.1038/nprot.2007.261>
91. Käll L, Canterbury JD, Weston J, Noble WS, MacCoss MJ. 2007. Semi-supervised learning for peptide identification from shotgun proteomics datasets. *Nat Methods* 4:923–925. <https://doi.org/10.1038/nmeth1113>